THE JOURNAL OF BIOLOGICAL CHEMISTRY VOL. 292, NO. 11, pp. 4484–4498, March 17, 2017

Nectin-like 4 Complexes with Choline Transporter-like Protein-1 and Regulates Schwann Cell Choline Homeostasis and Lipid Biogenesis *in Vitro*[*]

Received for publication, July 12, 2016, and in revised form, January 13, 2017 Published, JBC Papers in Press, January 24, 2017, DOI 10.1074/jbc.M116.747816

Corey Heffernan[‡], Mohit R. Jain[§], Tong Liu[§], Hyosung Kim[‡], Kevin Barretto[‡], Hong Li[§], and Patrice Maurel[‡1]

From the [‡]Department of Biological Sciences, Rutgers, the State University of New Jersey, Newark, New Jersey 07102-1814 and the [§]Center for Advanced Proteomics Research, New Jersey Medical School, Newark, New Jersey 07103

Edited by Dennis R. Voelker

Nectin-like 4 (NECL4, CADM4) is a Schwann cell-specific cell adhesion molecule that promotes axo-glial interactions. *In vitro* and *in vivo* studies have shown that NECL4 is necessary for proper peripheral nerve myelination. However, the molecular mechanisms that are regulated by NECL4 and affect peripheral myelination currently remain unclear. We used an *in vitro* approach to begin identifying some of the mechanisms that could explain NECL4 function. Using mass spectrometry and Western blotting techniques, we have identified choline transporter-like 1 (CTL1) as a putative complexing partner with NECL4. We show that intracellular choline levels are significantly elevated in NECL4-deficient Schwann cells. The analysis of extracellular d_9-choline uptake revealed a deficit in the amount of d_9-choline found inside NECL4-deficient Schwann cells, suggestive of either reduced transport capabilities or increased metabolization of transported choline. An extensive lipidomic screen of choline derivatives showed that total phosphatidylcholine and phosphatidylinositol (but not diacylglycerol or sphingomyelin) are significantly elevated in NECL4-deficient Schwann cells, particularly specific subspecies of phosphatidylcholine carrying very long polyunsaturated fatty acid chains. Finally, CTL1-deficient Schwann cells are significantly impaired in their ability to myelinate neurites *in vitro*. To our knowledge, this is the first demonstration of a *bona fide* cell adhesion molecule, NECL4, regulating choline homeostasis and lipid biogenesis. Phosphatidylcholines are major myelin phospholipids, and several phosphorylated phosphatidylinositol species are known to regulate key aspects of peripheral myelination. Furthermore, the biophysical properties imparted to plasma membranes are regulated by fatty acid chain profiles. Therefore, it will be important to translate these *in vitro* observations to *in vivo* studies of NECL4 and CTL1-deficient mice.

At the onset of peripheral myelination, the Schwann cell membrane encircles an axon to undertake "spiral wrapping." Continued migration of the inner Schwann cell membrane around the axon (under the outer membrane) forms multiple layers of overlying membrane (1). Lipid is deposited at the abaxonal and perinuclear aspects of the myelin segment for diffusion along the expanding membrane (2, 3). Compaction of all layers forms a mature myelin segment comprising ~70–85% lipid, by dry mass (4).

The myelin sheath also comprises 15–30% proteins (4). Myelin basic protein (MBP),[2] myelin protein zero (P0), and myelin proteolipid protein (PLP) represent the bulk of this small contribution of proteins and are important for compaction, maintenance, and function of the myelin sheath (5–7). Recently, we (8) and others (9, 10) described that Nectin-like 4 (NECL4, CADM4, TSLL2, and IGSF4C), a cell adhesion molecule that is expressed by Schwann cells, promotes axo-glial interaction along the internode and regulates PNS myelination *in vitro* and *in vivo*. Indeed, *in vitro* Schwann cell differentiation and myelination was inhibited in the absence of NECL4 (8). Similar results were obtained by perturbing axo-glial interactions with soluble forms of NECL4 and NECL4 ligand (10). These findings were supported by the delay in PNS myelination observed in the recently described NECL4 mouse knock-out (9). Although the NECL4$^{-/-}$ mice quickly recovered from the delay in the onset of myelination, they developed peripheral myelin that is morphologically abnormal, featuring focal hypermyelination and excessive myelin ensheathing multiple axons (9). NECL4 consists of three Ig ectodomains, a transmembrane domain, cytoplasmic FERM- and PDZ-binding domains that interact with scaffolding proteins (11, 12), and PDZ domain-containing proteins (13–15), respectively. Although NECL4

[*] This work was supported by NINDS Grants R01 NS065218 and R21 NS090305 from the National Institutes of Health (to P. M.) and by the Charles and Johanna Busch Memorial Fund at Rutgers, The State University of New Jersey. The authors declare that they have no conflicts of interest with the contents of this article. The content is solely the responsibility of the authors and does not necessarily represent the official views of the National Institutes of Health.

[1] To whom correspondence should be addressed: Dept. of Biological Sciences, Rutgers, The State University of New Jersey, Boyden Hall, Rm. 206, 195 University Ave., Newark, NJ 07102-1814. Tel.: 973-353-3489; Fax: 973-353-5712; E-mail: maurep01@andromeda.rutgers.edu.

[2] The abbreviations used are: MBP, myelin basic protein; CTL1, choline transporter-like 1; PLP, proteolipid protein; PEMT, phosphatidylethanolamine methyltransferase; qRT, quantitative RT; BisTris, 2-[bis(2-hydroxyethyl)-amino]-2-(hydroxymethyl)propane-1,3-diol; TEMED, *N*,*N*,*N*′,*N*′-tetramethylethylenediamine; DSP, dithiobis(succinimidyl propionate); coIP, co-immunoprecipitation; PFA, paraformaldehyde; PtdCho, phosphatidylcholine; PI(3,4,5)P_3, phosphatidylinositol 3,4,5-trisphosphate; PI(4,5)P_2, phosphatidylinositol 4,5-bisphosphate; PI(3,5)P_2, phosphatidylinositol 3,5-bisphosphate; PIP_3, phosphatidylinositol 3,4,5-trisphosphate; FL rescue, full-length rescue; PEMT, phosphatidylethanolamine methyltransferase; DSP, dithiobis(succinimidyl propionate); DRG, dorsal root ganglion; DAG, diacylglycerol; PTEN, phosphatase and tensin; NGF, neural growth factor; Fwd, forward; Rev, reverse; PNS, peripheral nervous system.

can potentially regulate the formation of multimeric protein complexes through cell-cell adhesion, the molecular mechanisms that are regulated by NECL4 and affect peripheral myelination currently remain unclear.

The most abundant lipids in myelin are cholesterol, galactocerebroside, sphingomyelin, and phosphatidylcholine (16). Some of these lipid species (phosphatidylcholine) are direct derivatives of intracellular choline, whereas the synthesis pathways of others (galactocerebroside) intersect with choline derivatives. The transfer of the phosphocholine group from cytidine diphosphocholine (CDP-choline) to diacylglycerol forms phosphatidylcholine (17). Through the enzymatic activity of phosphatidylcholine-specific phospholipase D, phosphatidylcholine is a source of phosphatidic acid (18), a short-lived phospholipid rapidly converted to diacylglycerol (18) or used in the synthesis of another important class of signaling and structural phospholipids, the phosphatidylinositols (19) and phosphorylated forms such as $PI(4,5)P_2$, $PI(3,4,5)P_3$, and $PI(3,5)P_2$. Sphingomyelin is produced by the action of sphingomyelin synthases that transfer the phosphocholine group of phosphatidylcholine to ceramide (20). Interestingly, sphingomyelin is also a source of ceramide (71, 72). Ceramide itself, through the action of the UDP-galactose-ceramide galactosyltransferase, is at the source of galactocerebroside, one of the most prominent sphingolipids in myelinating glial cells (21, 22).

Choline-derived lipids are important structural components as well as important reservoirs of signaling components that have a direct implication on the initiation of myelination, the compaction of the myelin sheath, and myelin maintenance. Although short lived, phosphatidic acid is an important signaling molecule that induces demyelination in the PNS via ERK pathway activation (23). Several phosphorylated phosphatidylinositol species (PIP_n) are critical to PNS myelination and myelin maintenance. For example, the conversion of $PI(4,5)P_2$ to $PI(3,4,5)P_3$ determines Schwann cell fate, *i.e.* ensheathing or myelinating (24, 25), and the levels of $PI(3,4,5)P_3$ regulate myelin thickness (26, 27). The negatively charged $PI(4,5)P_2$ interacts with the positively charged MBP to mediate a higher lipid order and condensation of the two apposing cytoplasmic leaflets (28–30). Furthermore, the disruption of the *Mtmr2* and *Fig4* genes, which tightly regulate the levels of $PI(3,5)P_2$, results in Charcot-Marie-Tooth type 4B (31) and 4J (32) phenotypes. It is interesting to note that the myelin abnormalities described in the NECL4 knock-out mouse (9) are similar to the *Mtmr2* knock-out mouse (31). Finally, sphingomyelin and cholesterol self-associate in the trans-Golgi network to form lipid rafts, and their fatty acid chains interact with membrane-bound myelin proteins PLP/DM2, MAL, CNP, and MOG (33–35). Therefore, sphingomyelin has an impact on the functionality of lipid rafts, the sorting and trafficking of myelin proteins (36, 37), as well as the assembly of signaling pathway platforms (38).

Eukaryotic cells possess a limited capability to synthesize choline *in situ*; thus choline is acquired from extracellular sources. Because of its positive charge, extracellular choline is transported via Solute Carrier (SLC) membrane transport proteins. The best characterized is SLC5A1, also known as the high-affinity choline transporter that transports choline into acetylcholine-synthesizing neurons (39). SLC44A1–5 or Choline Transporter-Like (CTL1–5) proteins form a family of intermediate-affinity choline transporters. CTL1 is expressed in oligodendroglia and neurons of the brain and spinal cord and along the internodes of myelinated peripheral nerve tracts (40–42). Notably, CTL1 is absent in non-myelinating tracts. CTL2–5 expression in the CNS is modest or absent, and their expression in the PNS remains unclear (42).

In our search to understand the mechanisms by which NECL4 regulates PNS myelination, we have uncovered a link between NECL4 and choline-dependent lipid metabolism. In this study, we report that, *in vitro*, levels of intracellular choline are increased in Schwann cells deficient in NECL4. Phosphatidylcholine and phosphatidylinositol levels are also significantly increased. We also show that NECL4 co-localizes and complexes with choline transporter-like 1 (CTL1). Finally, ablation of CTL1 expression in Schwann cells leads to a substantial decrease in myelin segment formation *in vitro*, in the Schwann cell-DRG neuron myelinating culture system.

Results

NECL4 Complexes with CTL1 in Schwann Cells—To start elucidating the mechanisms by which NECL4 regulates myelination, we performed proteomic mass spectrometry analyses on complexes co-immunoprecipitated with NECL4. In initial experiments, Schwann cells were treated with the cross-linker DSP. Because of its small size (12 Å), only proteins that are closely and non-randomly associated in a binding relationship are likely to become cross-linked with sufficient frequency to be detected. Upon Western blotting analysis of NECL4 immunoprecipitations, we observed a large (≈300 to ≥500 kDa) NECL4-positive complex, as well as accumulation of the NECL4-positive signal at the interface between the stacking and resolving gels suggestive of higher (>500 kDa) complexes (Fig. 1*A*, *cross-linked lane*, indicated *a*). Upon DTT-induced cleavage of the cross-links, the high molecular weight complexes disappeared, and monomeric NECL4 was detected at ~60 kDa (Fig. 1*A*, *reduced lane*, indicated *b*), further confirming NECL4 as a component of the larger molecular weight complexes. Among the proteins identified by LC-MS/MS from the NECL4-immunoprecipitated complexes excised from the gel shown in Fig. 1*A* (indicated *a*), SLC44A1, also known as CTL1, was consistently identified in repeated experiments. Fig. 1*B* shows a representative LC-MS/MS spectrum of a doubly charged ion (*m*/*z* 844.89) that corresponds to the CTL1 peptide ^{56}LVSGYDSYGNICGQR^{70} (*first peptide* indicated in *yellow* in Fig. 1*C*). The observed y- and b-ion series confirms the peptide sequence. Utilizing Scaffold Analysis software (43–45) with the Protein Threshold Identification and Peptide Threshold settings at 99.9 and 90% confidence, respectively, seven unique peptides representing 14% of the total CTL1 sequence were identified by LC-MS/MS (Fig. 1*C*, *yellow highlights*).

To confirm that NECL4 and CTL1 form a protein complex in Schwann cells, we performed non-cross-linked, reciprocal co-immunoprecipitations (coIP) from purified Schwann cell cultures with antibodies raised against NECL4 and CTL1 (Fig. 1*D*). CTL1 was detected from NECL4 immunoprecipitations and vice versa NECL4 was detected from CTL1 immunoprecipitations (Fig. 1*D, IP lanes*). Additional support for a NECL4-CTL1

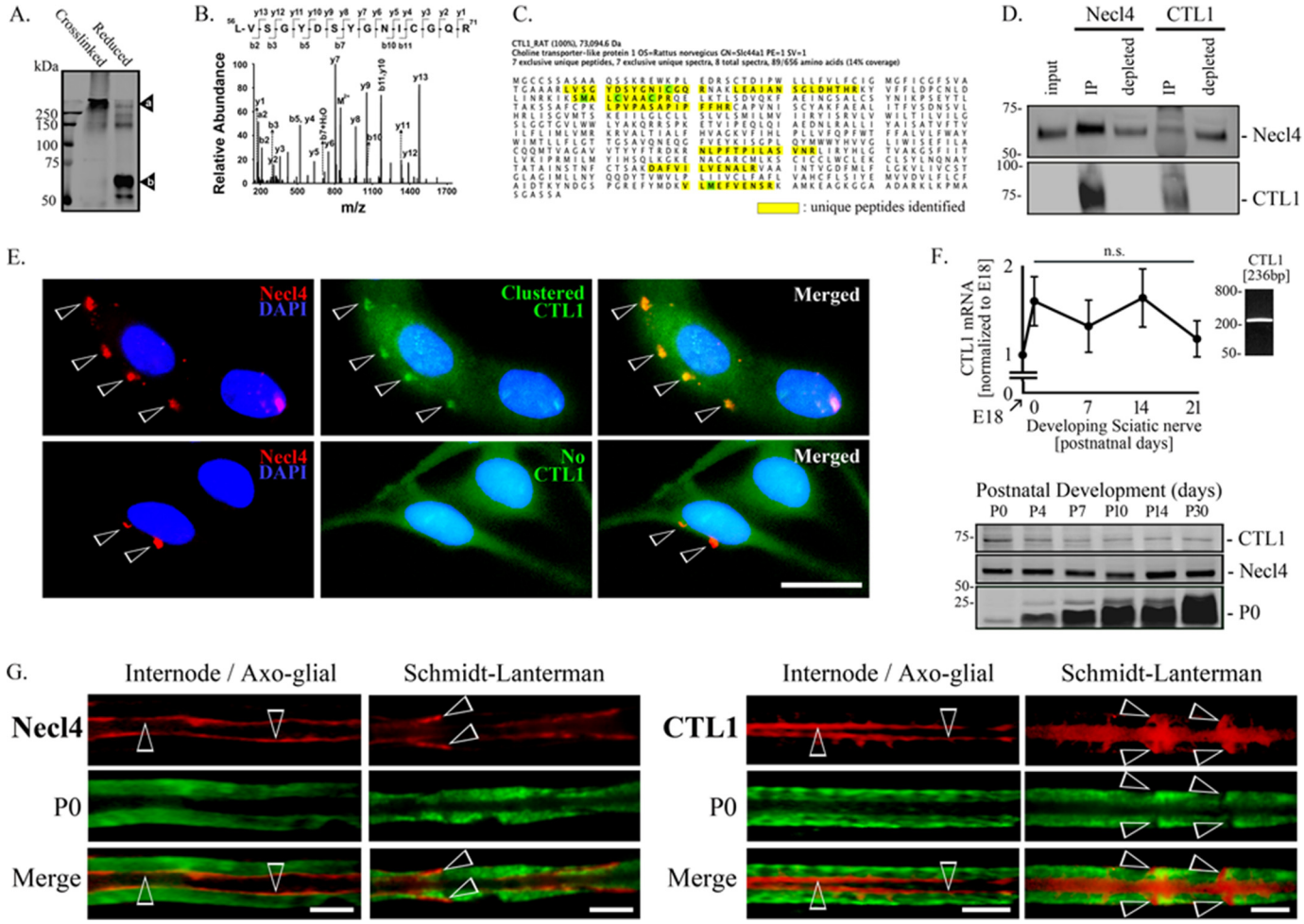

FIGURE 1. **NECL4 complexes with CTL1.** *A*, blotting of DSP cross-linked protein lysate for NECL4 highlighted a large molecular weight complex incorporating NECL4 (indicated by *a*). Following chemical reduction of the cross-link with DTT, we observed an enrichment in monomeric NECL4 (indicated by *b*) and loss of the large complex, confirming NECL4 as a complexing partner. *B*, LC-MS/MS spectrum of a doubly charged ion (*m/z* 844.89) that corresponds to the CTL1 peptide ^{56}LVSGYDSYGNICGQR^{70} (*1st peptide* highlighted in *yellow*, *C*). The observed y- and b-ion series confirm the peptide sequence. *C*, scaffold software analysis of LC-MS/MS data of co-immunoprecipitated complexes. Protein threshold identification and peptide threshold settings were set at 99.9 and 90% confidence, respectively. Seven unique peptides of CTL1 were identified, representing 14% of the total CTL1 sequence (*yellow highlights*). *D*, reciprocal pulldowns from Schwann cell lysates confirmed the complexing of NECL4 and CTL1. *E*, endogenous NECL4 was clustered with antibody before fixation and co-staining for CTL1. Co-localization of NECL4 and CTL1 after clustering (*top panels*) provides further evidence of the complexing of NECL4 and CTL1. Clusters are indicated at *arrowheads*. Absence of CTL1^{+} co-clusters with NECL4 when the CTL1 primary antibody was omitted (*bottom panels; no CTL1*) confirms the specificity of the co-clustering. *Scale bar,* 25 μm. *F*, quantitative RT-PCR for CTL1 in developing sciatic nerve (*top panel*; embryonic day E18.5 and postnatal days P0, P7, P14, and P21). Results are normalized to stage E18.5. Polyacrylamide gel electrophoresis of the qPCR amplicon revealed a unique band of the expected size for CTL1 (236 bp; see *inset*). CTL1 and NECL4 proteins are expressed in developing (myelinating) postnatal rat sciatic nerve (*bottom panel*; postnatal days P0–P30). *n.s.,* not significant. *G,* adult rat sciatic nerves were manually teased before labeling with NECL4 or CTL1 and P0 antibody. Both NECL4 and CTL1 localize to the Schwann internode/axo-glial interface (*arrowheads*) and Schmidt-Lanterman incisures (*arrowheads*). *Scale bars,* 5 μm.

complex was provided by co-clustering experiments. NECL4 was first clustered in live Schwann cells with a NECL4-specific antibody, followed by fixation and immunostaining for CTL1. Confocal microscopy analysis showed the co-localization of CTL1 with NECL4 clusters (Fig. 1*E*, *arrowheads*), providing further supporting evidence that, in Schwann cells, NECL4 and CTL1 form a protein complex. Similarly, immunostaining of adult rat teased sciatic nerves shows that CTL1 and NECL4 are both expressed along the myelinated internode, both localizing along the axo-glial interface and to the Schmidt-Lanterman incisures (Fig. 1*G*).

Quantitative RT-PCR (qRT-PCR) analysis (Fig. 1*F*, *top panel*) detected a unique band of the expected size for CTL1 (236 bp) expressed at a relatively constant level throughout the period of active myelination (postnatal days p0 to p21). CTL1 expression was further confirmed by Western blotting (Fig. 1*F*, *bottom panel*). P0 was used as a marker of ongoing myelination.

Taken together, these results suggest NECL4 and CTL1 form a protein complex in isolated as well as myelinating Schwann cells.

Choline Homeostasis Is Disrupted in NECL4-deficient Schwann Cells—Mammalian cells have a limited capability to synthesize choline, so the bulk of choline must be provided from the diet. Being a positively charged quaternary ammonium, choline requires active transport through the plasma membrane. The interaction between NECL4 and CTL1 prompted us to evaluate whether NECL4 might be regulating intracellular levels of choline in Schwann cells. NECL4 was knocked down in Schwann cells using shNECL4 constructs previously described in Maurel *et al.* (8). To corroborate the specificity of the NECL4 knock-

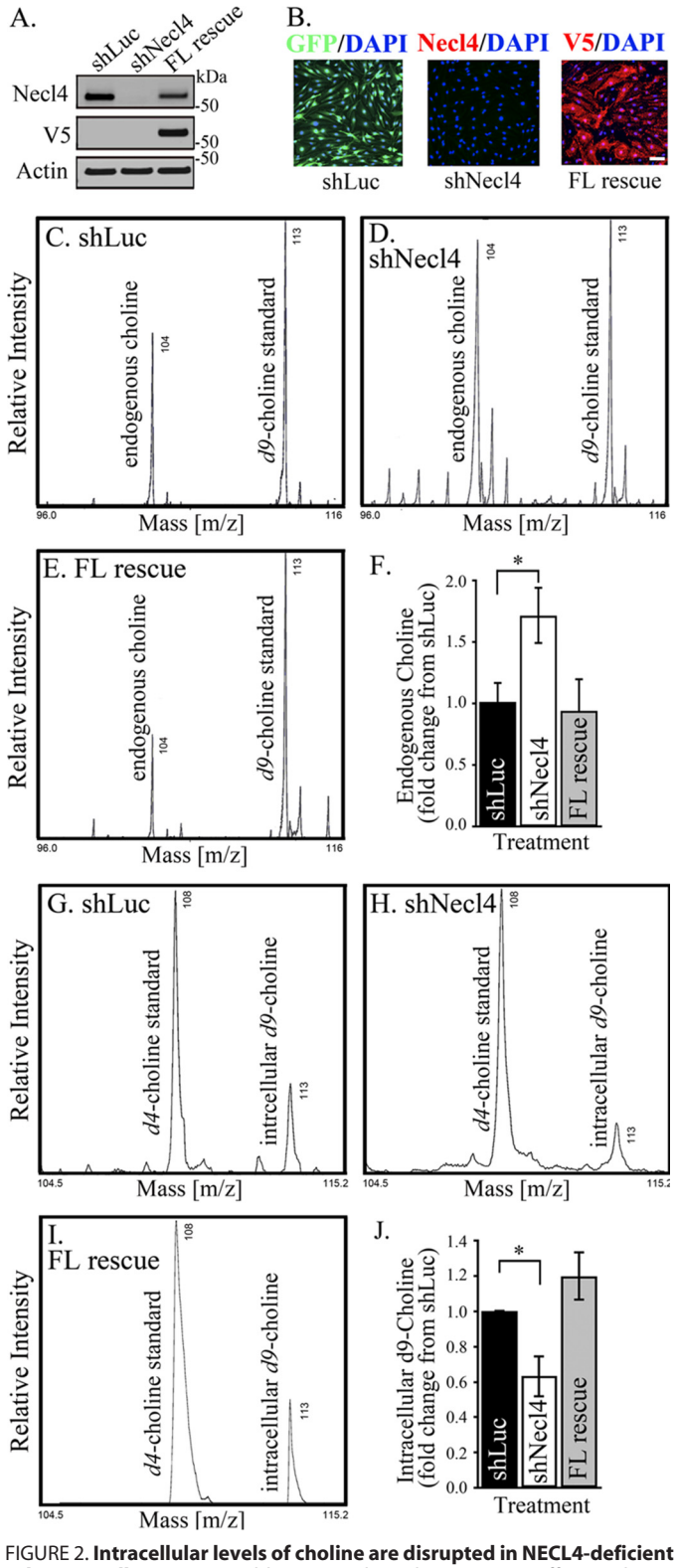

FIGURE 2. **Intracellular levels of choline are disrupted in NECL4-deficient Schwann cells.** *A*, Western blotting analysis demonstrates efficient shRNA knockdown of NECL4 (*top blot*) and expression of V5-tagged NECL4 rescue construct (*V5*, *middle blot*). *B*, immunocytochemical labeling of infected cells demonstrates efficient (>90%) infection of Schwann cells with the shLuc construct (*left image,* ascertained by GFP expression), confirmation of complete knockdown of NECL4 (*middle image*), and efficient expression of the FL rescue construct (*right image,* ascertained by V5 labeling). *Scale bar,* 50 μm. *C–F*, intracellular choline in shLuc (*C*), shNECL4 (*D*), and FL rescue (*E*) Schwann cells was assessed by MALDI-TOF mass spectrometry. For comparative analysis, spectral peaks of intracellular choline (*m/z* 104) were normalized to d_9-choline standard spectral peaks (*m/z* 113). Intracellular choline was significantly elevated in NECL4-deficient Schwann cells (compare intracellular choline spectral peaks of shLuc and shNECL4). Quantitation in *F* depicts mean ± S.E. of $n = 4$ independent experiments, *, $p < 0.05$. *G–J,* intracellular levels of d_9-choline after uptake from the extracellular culture media by NECL4-deficient Schwann cells was significantly lower (compare *intracellular* d_9*-choline* spectral peaks in shLuc control (*G*) with *NECL4*-deficient Schwann cells (*H*). Deuterated d_4-choline (*m/z* 108) was used as a common standard. *J*, quantitation depicts mean ± S.E. of $n = 4$ independent experiments, *, $p < 0.05$.

down effects and to exclude nonspecific off-target effects on choline transport and intracellular levels, we also performed knockdown rescue experiments (FL rescue) in which an shRNA-resistant V5-tagged NECL4 construct is reintroduced in NECL4-deficient Schwann cells. Controls were Schwann cells infected with the luciferase shRNA construct (shLuc). Western blotting analyses (Fig. 2*A*) confirmed the efficient knockdown ("shNECL4") as well as re-expression of NECL4 (FL rescue; confirmed by V5 blotting) in Schwann cells. Immunocytochemical staining (Fig. 2*B*) demonstrated the ablation of NECL4 and the re-expression of the (V5-tagged) full-length rescue construct in >90% of Schwann cells (Fig. 2*B*). Immunostaining for GFP also showed a similar rate of expression (>90%) of the shLuc control construct by Schwann cells.

The abundance of endogenous intracellular choline in Schwann cells was determined by MALDI-TOF mass spectrometry (Fig. 2, *C–F*). For comparative assessment between experimental conditions, deuterated d_9-choline (labeled "d_9-choline standard") was added to the common matrix into which all methanol-extracted Schwann cells were prepared, crystallized and spotted. Ratios of intracellular choline to d_9-choline standard (by % relative intensity) revealed a significant 75% increase in intracellular choline in NECL4-deficient Schwann cells (Fig. 2, *C, D* and *F*). Intracellular choline returned to control levels in Schwann cells rescued with full-length NECL4 (Fig. 2, *E* and *F*), underscoring the specificity of the results.

We also performed uptake experiments by adding d_9-choline to shLuc and shNECL4 Schwann cell cultures (with and without NECL4 rescue) and assessed the levels of intracellular d_9-choline by MALDI-TOF (Fig. 2, *G–J*). Similarly to the above, deuterated d_4-choline was added to the common matrix to serve as a comparative control. We observed a significant decrease (≈35%) in intracellular d_9-choline in NECL4-deficient Schwann cells compared with shLuc Schwann cells (Fig. 2,*G, H,* and *J*). Intracellular levels of d_9-choline returned to control levels in Schwann cells rescued with full-length NECL4 (Fig. 2, *E* and *F*). Intracellular d_9-choline was comparable with control levels in Schwann cells that were rescued with full-length NECL4 (Fig. 2, *I* and *J*), which underscores the specificity of the results.

Taken together, these results suggest a dysregulation of choline homeostasis in NECL4-deficient Schwann cells. Although the uptake data may suggest an inability of NECL4-deficient Schwann cells to transport extracellular choline into the cytosol, they may also reflect an increase in the metabolic transformation of intracellular choline.

Phosphatidylcholine Levels, as Well as Fatty Acid Chain Length and Unsaturation, Are Disrupted in NECL4-deficient Schwann Cells—Phosphatidylcholines are a major class of phospholipids that use choline as the headgroup attached to the glycerophosphoric acid. They are abundant in cells' plasma

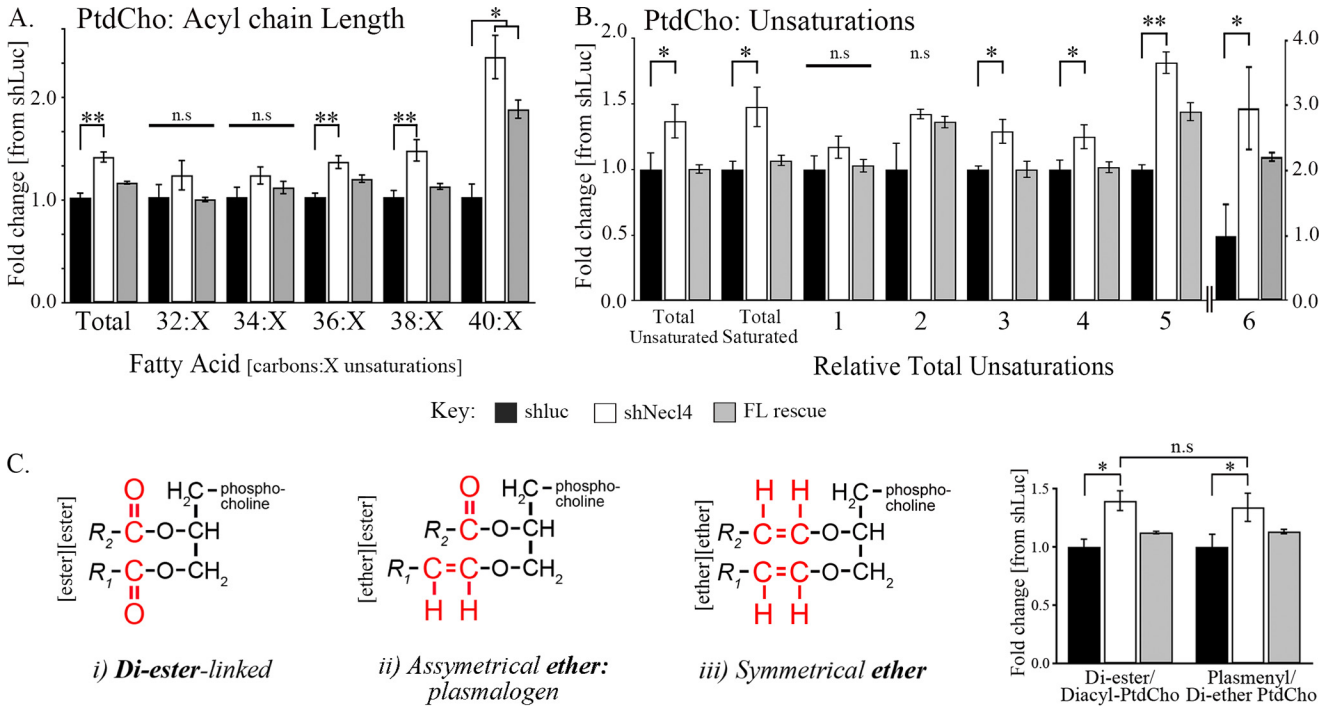

FIGURE 3. **Phosphatidylcholine profile (acyl chain length and unsaturation) is disrupted in NECL4-deficient Schwann cells.** *A*, relative abundance of total PtdCho and specific PtdCho subspecies of given fatty acyl chain length (32:*X*–40:*X*; *X* denotes any unsaturation) between shLuc, shNECL4 and FL rescue constructs. Total phosphatidylcholine and numerous subspecies were significantly elevated in NECL4-deficient Schwann cells. Mean ± S.E. of $n = 5$ independent experiments is depicted (*, $p < 0.05$; **, $p < 0.01$, *n.s.*, not significant). *B*, relative abundance of total unsaturated and saturated phosphatidylcholine, and specific subspecies incorporating one to five unsaturations (*left axis*) and six unsaturations (*right axis*), regardless of acyl chain length. Total unsaturated and saturated phosphatidylcholine and phosphatidylcholine species of three to six unsaturations were significantly elevated in NECL4-deficient Schwann cells. *C, panels i–iii*, diagrammatic representation of ester- and ether-linked (asymmetrical/plasmalogen, and symmetrical) phosphatidylcholine. Ester- and ether-linked phosphatidylcholine species are similarly elevated in NECL4-deficient Schwann cells. Mean ± S.E. of $n = 5$ independent experiments is depicted (*, $p < 0.05$, *n.s.*, not significant).

membrane and in the myelin sheath. Because intracellular choline levels were disrupted in NECL4-deficient Schwann cells, we used liquid chromatography coupled to mass spectrometry (LC-MS/MS) to assess the abundance of phosphatidylcholine in these cells, as well as in NECL4-rescued Schwann cells. The results presented in Fig. 3 are expressed in fold of change relative to control (shLuc) Schwann cells. Concurrent with the increase in choline within NECL4-deficient Schwann cells, we observed a significant increase (≈45%; $p < 0.01$) in total phosphatidylcholine (Fig. 3*A*, *PtdCho, Total*). Total phosphatidylcholine levels returned to control levels in NECL4-rescued Schwann cells.

The length (measured in the number of carbons) and unsaturation profile of the two fatty acid chains, which are also linked to the glycerophosphoric acid group, account for the large diversity in phosphatidylcholines. Using the LC-MS/MS approach, we reliably detected 65 individual species of phosphatidylcholine, with the combined length of the two fatty acid chains ranging from 30 to 40 carbons (Fig. 3*A*) and up to six unsaturations (Fig. 3*B*). Phosphatidylcholine species with overall fatty acid chains of 36:*X* and 38:*X* carbons (*X* denotes any un/saturation) were significantly increased by about 40–50% (Fig. 3*A*; $p < 0.01$) in Schwann cells lacking NECL4. The re-expression of the full-length NECL4 construct completely rescued this effect. Interestingly, the levels of phosphatidylcholine species with overall fatty acid chains of 40 carbons (40:*X*) were most affected, with a dramatic 150% increase compared with controls (Fig. 3*A*). The re-expression of NECL4 did not fully rescue the phenotype, and the levels of phosphatidylcholine 40:*X* remained significantly elevated in the rescued Schwann cells. We did not observe significant differences in phosphatidylcholine 32:*X* and 34:*X* levels between the control, knockdown, and rescue groups.

We further investigated whether the extent of phosphatidylcholine fatty acid chain (un)saturation was affected in NECL4-deficient Schwann cells (Fig. 3*B*). The pools of only saturated and only unsaturated phosphatidylcholine were both significantly and similarly elevated (≈35–50%) in NECL4-deficient Schwann cells compared with shLuc controls. The levels were comparable with controls after full-length NECL4 rescue (Fig. 3*B*). A more detailed analysis showed that phosphatidylcholine carrying fatty acid chains with 5 and 6 unsaturations represent the species most increased (up to 75 and 300%, respectively), followed by phosphatidylcholine carrying fatty acid chains with 3 and 4 unsaturations (up about 20%; Fig. 3*B*). The levels of phosphatidylcholine with 1 or 2 unsaturations were not significantly affected (Fig. 3*B*).

The glycerophosphocholine headgroup of phosphatidylcholine forms either ester or ether linkages to fatty acids (Fig. 3*C*). Ether-linked phosphatidylcholine species can be symmetrical (di-ether) or asymmetrical (an ether- and ester-linked fatty acid chain, as for plasmalogens; Fig. 3*C, panels i–iii*); we pooled the as/symmetrical ether-linked phosphatidylcholine species for comparison with ester-linked phosphatidylcholine. We de-

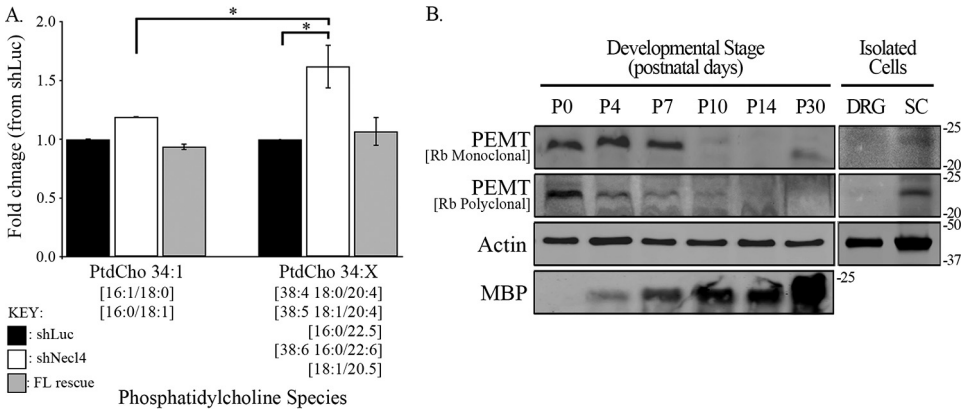

FIGURE 4. **Lipids associated with synthesis via the PEMT pathway are significantly elevated in NECL4-deficient Schwann cells *in vitro*, and PEMT is expressed in myelinating sciatic nerves.** *A*, comparison of PtdCho species associated with synthesis via CDP:choline pathway (34:1) and PEMT synthetic pathway (38:4, 38:5, and 38:6) (47). We observed a significant over-representation of lipids associated with synthesis via the PEMT pathway than those via the CDP:choline pathway. *B,* Western blotting analysis of PEMT expression in developing (myelinating) sciatic nerve (postnatal days P0 to P30) and in isolated Schwann cells and DRG neurons, using two independent anti-PEMT antibodies (anti-rabbit monoclonal, *top panel*; anti-rabbit polyclonal, *2nd from top*). Both antibodies easily detected PEMT during the early stages of myelination (P0 to P7). Detection dropped sharply at P10, and PEMT was no longer detectable from p14 onward. PEMT is primarily expressed by Schwann cells (*SC*) and was not detected in DRG neurons.

tected various subspecies of ester-linked ($n = 19$) and ether-linked ($n = 12$) phosphatidylcholine species in Schwann cells. Similar to total phosphatidylcholine, both groups were significantly ($p < 0.01$) but comparably ($p > 0.05$) elevated in NECL4-deficient Schwann cells compared with shLuc controls and were rescued by re-expressing NECL4 (Fig. 3*C*). These results suggest that NECL4 regulates (directly or indirectly) the abundance of phosphatidylcholine proper and not selectively for ester- or ether-linked subspecies.

Phosphatidylcholine species of 16–18 carbon chains with little or no unsaturation (*e.g.* 16:0/18:1 and 18:1/18:1) are commonly synthesized directly from CDP-choline via the Kennedy pathway (17). Phosphatidylcholine species synthesized via the phosphatidylethanolamine methyltransferase (PEMT) pathway (46) are commonly characterized by considerably longer fatty acid chains with higher unsaturation, such as 18:0/20:4, 18:1/20:4, 18:0/22:4, or 18:1/20:6 (47, 48). Therefore, the dramatic increase in overall fatty acid chain length and unsaturation prompted us to analyze for specific phosphatidylcholine species carrying long chain polyunsaturated fatty acid chains (PUFA), such as 20:4 or 22:6. As shown in Fig. 4*A*, whereas phosphatidylcholines with fatty acid chains of 16–18 carbons with no or little unsaturation were not overtly affected by NECL4 (≈20%; $p < 0.05$), the representation of phosphatidylcholine species carrying 20:4 and 22:6 fatty acid chains was dramatically increased (≈60%) in NECL4-deficient Schwann cells ($p < 0.05$). Using two independent anti-PEMT antibodies (rabbit monoclonal against the C terminus of PEMT; rabbit polyclonal against full-length PEMT) to perform Western blotting analyses of developing sciatic nerves (Fig. 4*B*; postnatal days P–P30), PEMT was easily detected during the 1st week (P0–P7) of postnatal development. PEMT was below detection levels from thereon (P14 to P30). We also assessed lysates of purified Schwann cells (Fig. 4, *SC*) and dorsal root ganglia neurons (Fig. 4, *DRG*) to determine the cell type expression of PEMT. Both antibodies detected PEMT exclusively in Schwann cell lysate, and not in DRG lysate. Taken together, these results suggest that PEMT is expressed at the onset of myelination in the developing sciatic nerve and primarily in myelinating Schwann cells.

Phosphatidylinositol Levels, as Well as Fatty Acid Chain Length and Unsaturation, Are Disrupted in NECL4-deficient Schwann Cells—Phosphatidylcholine is an important source of phosphatidic acid (18), which is quickly converted to diacylglycerol or used in the synthesis of phosphatidylinositols. Because some phosphorylated derivatives of phosphatidylinositols have been shown to be important to PNS myelination (for example, $PI(3,4,5)P_3$ and $PI(3,5)P_2$), we furthered our LC-MS/MS analysis to the levels and profile of phosphatidylinositols (Fig. 5). We reliably detected 45 individual phosphatidylinositol species with fatty acid chain lengths totaling 32–40 carbons. As with phosphatidylcholine, the overall levels of phosphatidylinositols were significantly increased, albeit to a lesser extent (about 25%, Fig. 5*A*) in NECL4-deficient Schwann cells, relative to shLuc controls. This increase particularly affected phosphatidylinositol species 34:*X* and 36:*X* (Fig. 5*A*, $p < 0.05$), whereas species 38:*X* and 40:*X* were not significantly increased. Re-expression of full-length NECL4 completely rescued the levels of total phosphatidylinositols, specifically species 34:*X* and 36:*X*.

All the detected phosphatidylinositol species were unsaturated to varying degrees (Fig. 5*B*). A detailed analysis showed that the knockdown of NECL4 resulted in significantly elevated phosphatidylinositol species with fatty acids carrying two and three unsaturations (Fig. 5*B*), whereas the levels of phosphatidylinositol species with one and four to six unsaturations were variable and not significantly different between all Schwann cell conditions (Fig. 5*B*). Re-expression of full-length NECL4 rescued phosphatidylinositol species with two unsaturations but did not rescue the elevated level of phosphatidylinositol species with three unsaturations.

Phosphorylated phosphatidylinositols are difficult to ionize, and we were unfortunately not able to further our analysis to species such as $PI(3,4,5)P_3$ (relevant to the ensheathing/myelinating phenotype transition, as well as myelin thickness in the PNS) and $PI(3,5)P_2$ (relevant to the Charcot-Marie-Tooth type 4B-like phenotype observed in the NECL4 knock-out mouse).

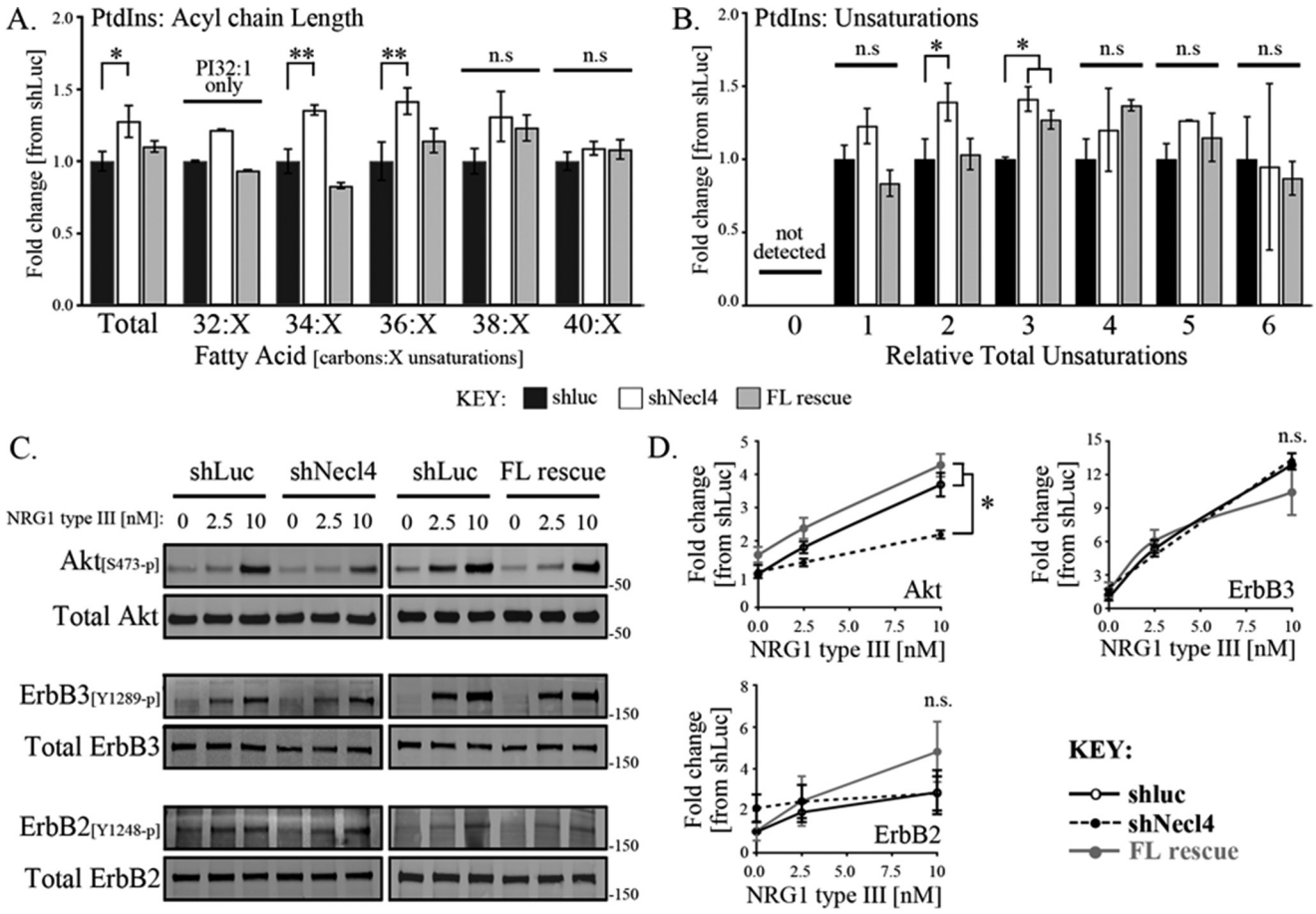

FIGURE 5. **Phosphatidylinositol profile (acyl chain length and unsaturation) and phosphatidylinositol-dependent intracellular signaling in NECL4-deficient Schwann cells.** *A*, relative abundance of total phosphatidylinositol (*PtdIns*) and specific phosphatidylinositol subspecies of given fatty acyl chain length (32:*X*–40:*X*; *X* denotes any unsaturations) between shLuc, shNECL4 and FL rescue constructs. Total phosphatidylinositol and 34:*X* and 36:*X* subspecies were significantly elevated in NECL4-deficient Schwann cells. *B*, relative abundance of total saturated phosphatidylinositol (not detected) and specific unsaturated subspecies incorporating one to five unsaturations (regardless of acyl chain length). Phosphatidylinositol species of two to three unsaturations were significantly elevated in NECL4-deficient Schwann cells. Mean ± S.E. of $n = 5$ independent experiments is depicted (*, $p < 0.05$; **, $p < 0.01$, *n.s.*, not significant). *C*, ERBB/PI3K/AKT pathway was stimulated in NECL4-deficient Schwann cells and controls with application of a soluble form of type III Nrg1β1 and the phospho-activation of ERBB3, ERBB2, and AKT assessed by quantitative Western blotting. The activation of AKT was significantly repressed in NECL4-deficient Schwann cells compared with controls, independent of fluctuations in upstream ErbB2 or ErbB3 activation. *D*, quantitation (Odyssey imaging system, LI-COR) of Western blottings in *C*. Mean ± S.E. of ratios of phospho-protein/total (AKT ERBB2 and ERBB3) protein of $n = 4–8$ independent experiments are depicted (*, $p < 0.05$).

To provide preliminary evidence that disruptions to the level and profile of phosphatidylinositols may affect phosphatidylinositol-dependent intracellular signaling, we used a soluble form of type III neuregulin-1 (Nrg1) and quantitative Western blotting for phospho-AKT (Ser^{473}), phospho-ERBB2 (Tyr^{1248}), and phospho-ERBB3 (Tyr^{1289}) to determine the activation of the ERBB/PI3K/AKT pathway in shLuc control, NECL4-deficient, and NECL4-rescued Schwann cells (Fig. 5, *C* and *D*). Nrg1-mediated activation of AKT was significantly repressed in Schwann cells lacking NECL4 compared with controls (compare 10 nM Nrg1 conditions in shLuc and shNECL4; *upper blots*, Fig. 5, *C* and *D*) and was rescued upon re-expression of NECL4. The phosphorylation of upstream ERBB2 and ERBB3 was not affected, suggesting that the deficit in AKT activation was not attributable to repressed activation ERBB2 or ERBB3 (*lower blots,* Fig. 5, *C* and *D*).

Diacylglycerol (DAG) and Sphingomyelin Levels and Profiles Are Largely Unaffected by the Presence or Absence of NECL4—Phosphatidylcholine is also a precursor to the biosynthesis of sphingomyelin, generating diacylglycerol in the process (20). Total levels of diacylglycerol, and individual species 32–40 carbon fatty acid chains, were unchanged between all groups (control, NECL4-deficient, and NECL4-rescued Schwann cells; Fig. 6*A*). Although we did observe a significant reduction in total unsaturated diacylglycerol species and a significant increase in diacylglycerol species of four unsaturations, diacylglycerols species of none to three unsaturations were unaffected by NECL4 (Fig. 6*B*). Diacylglycerol species of five to six unsaturations were not detected (Fig. 6*B*). Of the 34 sphingomyelin subspecies detected, with fatty acid chains of 14–26 total carbons and none to two unsaturations, no significant differences were observed in total abundance or subspecies of sphingomyelin (Fig. 6, *C* and *D*). Sphingomyelin species of three to six unsaturations were not detected (Fig. 6*D*).

In Vitro Myelination Is Significantly Inhibited in CTL1-deficient Schwann Cells—To characterize the impact of CTL1 in regulating myelination, we designed two short hairpin RNAs directed against distinct sequences within CTL1 (shCTL1A and shCTL1B). An shRNA targeting luciferase (shLuc) served as a nonspecific target control. The corresponding sequences

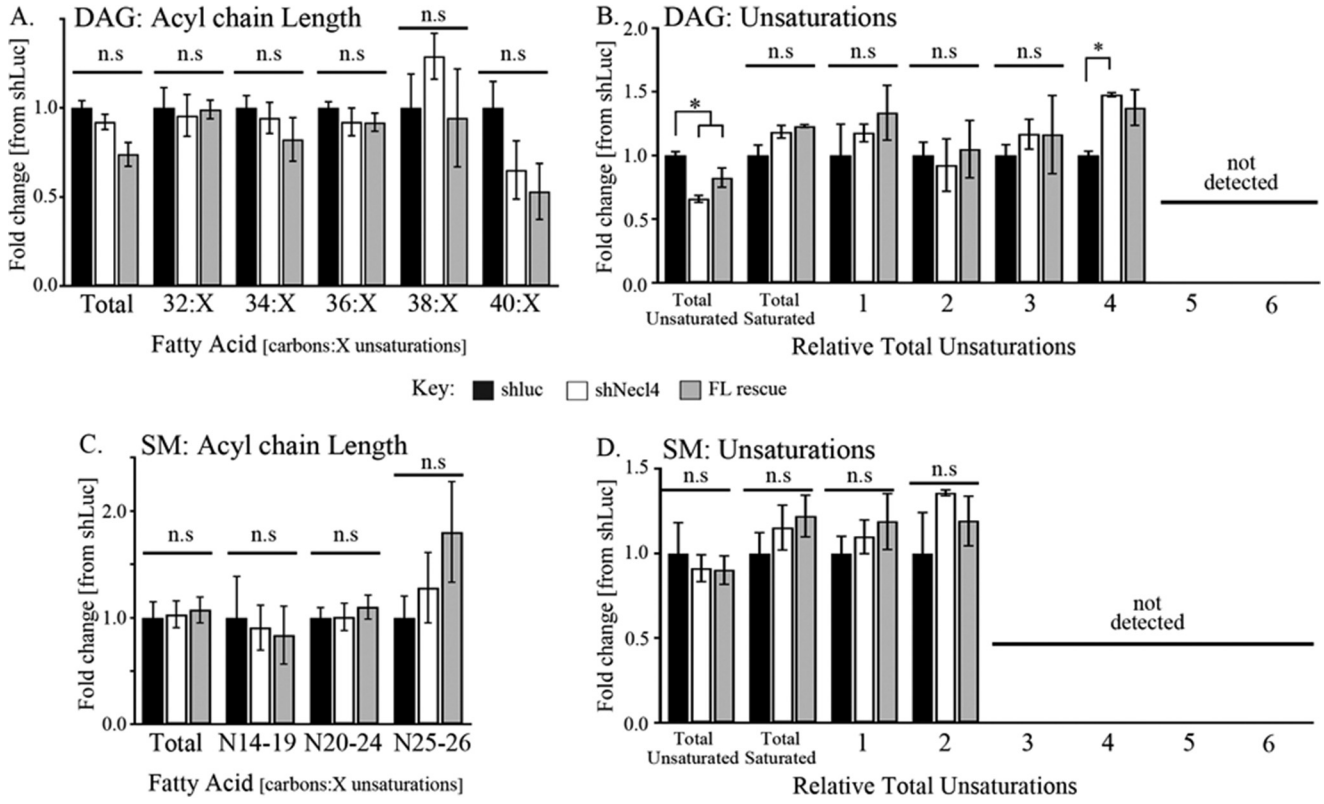

FIGURE 6. **Acyl chain length and unsaturation profiles of diacylglycerol (*A* and *B*) and sphingomyelin (*C* and *D*) are largely unaffected by the presence or absence of NECL4.** *A*, relative abundance of total diacylglycerol (*DAG*) and specific DAG subspecies of given fatty acyl chain length (32:*X*–40:*X*; *X* denotes any unsaturation) between shLuc, shNECL4, and FL rescue constructs. Total DAG and abundance of specific subspecies were unaffected in NECL4-deficient Schwann cells. Mean ± S.E. of $n = 5$ independent experiments is depicted (*n.s.*, not significant). *B*, one to six unsaturations, regardless of acyl chain length. Although total unsaturated DAG was significantly reduced, and DAG (four unsaturations) was elevated, in NECL4-deficient Schwann cells, DAG species of none to three unsaturations were unaffected. Mean ± S.E. of $n = 5$ independent experiments is depicted (*, $p < 0.05$, *n.s.*, not significant). *C* and *D*, relative abundance of sphingomyelin (*C*; total, and subspecies of 14–26 carbon fatty acids) and (un)saturated fatty acid profile (*D*) were unaffected by the presence or absence of NECL4.

were cloned into the pLL3.7 vector (49) for lentiviral transduction of purified Schwann cells. All constructs co-expressed GFP whose immunodetection confirmed the infection of >90% of Schwann cells (Fig. 7*A*). Western blotting analyses confirmed the efficient knockdown of CTL1 expression in Schwann cells (Fig. 7*B*) by both shCTL1 constructs. Infected Schwann cells were then plated to purified DRG neuron cultures and maintained under myelinating conditions for 10 days before immunostaining for MBP to detect compact myelin segments. The knockdown of CTL1 in Schwann cells significantly impaired the formation of myelin segments compared with shLuc controls (Fig. 7*C*). Quantitation demonstrated a significant reduction of about 70% in the number of MBP-positive myelin segments (Fig. 7*D*). At 434 ± 5, 421 ± 7, and 431 ± 6 DAPI-stained nuclei per field of view (shLuc, shCTL1A, and shCTL1B, respectively), Schwann cell density in the co-culture system was not affected by the knockdown of CTL1 expression. No psychotic nuclei were also observed. Taken together, these results suggest that CTL1 is a positive regulator of Schwann cell myelination, independently of Schwann cell proliferation and/or survival.

Discussion

In the PNS, NECL4 is a Schwann cell-specific cell adhesion molecule that promotes axo-glial interaction along the myelinated internode by interacting with its axonal cell adhesion molecule counterpart NECl1 (8, 10). *In vitro* studies have demonstrated that NECL4 is needed for myelination (8, 10), and the delay in the onset of myelination observed in the *in vivo* NECL4$^{-/-}$ mouse supports that finding (9). Most dramatic are the morphological abnormalities observed at 2 months of age, in particular focal hypermyelination with tomacula and myelin outfoldings that are characteristic of Charcot-Marie-Tooth neuropathies (9, 50). In this study, we describe the complexing of NECL4 with CTL1 and the impact of NECL4 deficiency on choline-dependent metabolism in purified Schwann cells. We discuss how these results may provide a molecular basis to some of the abnormalities observed in the PNS myelin of the NECL4$^{-/-}$ mouse, and we further outline some of the questions that they raise.

The mechanisms by which NECL4 regulates myelination remain to be elucidated. However, the presence of FERM- and PDZ-binding domains in the cytoplasmic tail of NECL4 strongly suggests that its likely function is to form and stabilize multiprotein complexes along the adaxonal membrane and the Schmidt-Lanterman incisures. To characterize NECL4-binding partners, we performed mass spectrometry analyses of NECL4 coIPed complexes and identified CTL1 as a potential partner for NECL4 (Fig. 1, *A*–*C*). This result was corroborated

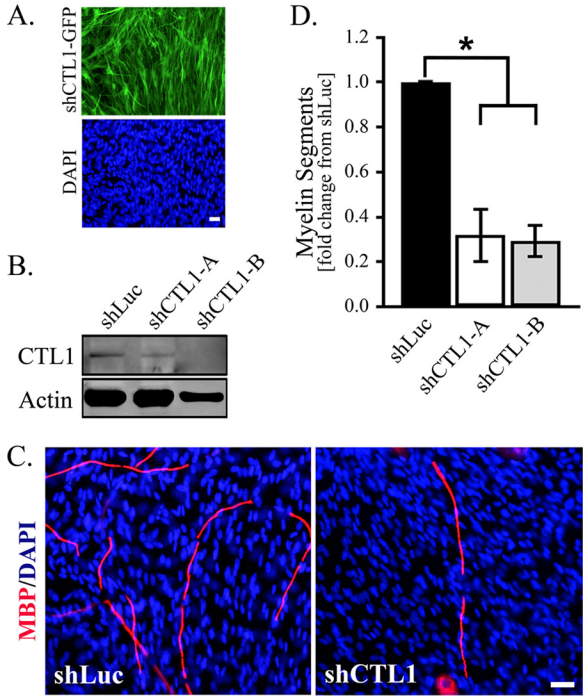

FIGURE 7. **CTL1-deficient Schwann cells are significantly impaired in their ability to form mature MBP$^+$ myelin segments *in vitro*.** *A*, immunocytochemical staining confirms efficient infection of Schwann cells with shCTL1 (co-expressing GFP) prior to plating to DRG neurite cultures. *B*, Western blot confirms efficient shRNA-mediated knockdown of CTL1 in Schwann cells with two different shRNA constructs (shCTL1A and shCTL1B) before plating to DRG. *C*, CTL1-deficient Schwann cells (or shLuc controls) were co-cultured with DRG for 10 days in myelinating conditions before immunocytochemistry labeling for MBP (*red*; for myelin segments) and nuclei (DAPI). We observed significantly fewer MBP^{2+} myelin segments in Schwann cell expressing either shRNA construct compared with shLuc controls. *Scale bar,* 50 μm. *D*, quantitation of MBP$^+$ myelin segments in shLuc, shCTL1A, and shCTL1B from $n = 3$ experiments. Mean $\pm$ S.E. depicted, *, $p < 0.05$.

by reciprocal co-immunoprecipitations and Western blotting detection (Fig. 1*D*) and by the co-localization of CTL1 with NECL4 after antibody-mediated clustering of NECL4 (Fig. 1*E*) and immunofluorescent staining of adult sciatic nerve (Fig. 1*G*). This latter result implies a physiological interaction, direct or indirect, between endogenous NECL4 and CTL1 in live Schwann cells, which would preclude the detection of a spurious interaction in the Schwann cell lysates of the coIP experiments. Finally, although the presence of CTL1 on axons cannot be excluded, the overlapping pattern of expression of CTL1 with NECL4 in mature nerves (Fig. 1*G*) along the axo-glial junction and in the Schmidt-Lanterman clefts further supports an interaction between NECL4 and CTL1.

The interaction between NECL4 and CTL1 suggested that choline homeostasis and/or choline-dependent metabolism might be affected in NECL4-deficient Schwann cells. Indeed, we detected a significant increase (75%) in intracellular choline in NECL4-deficient cells (Fig. 2, *C–F*). Interestingly, however, lower amounts of extracellular d_9-choline were found in the cytosol of NECL4-deficient Schwann cells (Fig. 2, *G–J*) compared with controls, in extracellular d_9-choline uptake experiments. Although this result, in association with the NECL4-CTL1 interaction, may suggest that there is a deficit in choline transport in NECL4-deficient Schwann cells, the methodological approach that we used does not allow us to make a definitive conclusion at this time. Indeed, choline could be quickly metabolized once transported inside the cells, and the decreased amount of intracellular d_9-choline in the absence of NECL4 may reflect an increase in the transformation of choline into phosphocholine and/or betaine. Notwithstanding, these results on intracellular choline demonstrate in Schwann cells a dysregulation of choline homeostasis in the absence of NECL4.

Concomitant with the increase in intracellular choline, we also observed a significant increase (50%) in its derivative, phosphatidylcholine (Fig. 3). Phosphatidylcholine species 36:*X* and 38:*X* were similarly increased (40 and 50%, respectively), whereas phosphatidylcholine 40:*X* was the most significantly increased (over 2.5-fold). No significant difference was noted for phosphatidylcholine 32:*X* and 34:*X*. The glycerol moiety of phosphatidylcholine forms either ester or ether bonds to fatty acid chains (*outlined,* Fig. 3*C*). The ether bond is mostly present in plasmalogens (particularly abundant in the myelin sheath (51)). Ether-phosphatidylcholine and di-ester-phosphatidylcholine species were similarly enriched in NECL4-deficient Schwann cells (Fig. 3*C*). Altogether, these results suggest that NECL4 mostly regulates the levels of the total pool of phosphatidylcholine, agreeing with the concomitant increase in intracellular choline levels and not selectively for ester- or ether-linked species. It is possible, however, that the increase in overall phosphatidylcholine impacts the representation of certain fatty acid chains. This is particularly noticeable with the dramatic increase in phosphatidylcholine with fatty acid chains totaling 40 carbons (150% increase *versus* 40–50% for all other species; Fig. 3*A*) and the dramatic increase in phosphatidylcholine with fatty acid chains carrying five to six unsaturations (75–300% increase *versus* 0–25% for all other species; Fig. 3*B*).

The deposition of excess unsaturated phosphatidylcholine (Fig. 3*B*) in the Schwann cell membrane may promote excessive membrane curvature (52) and reduced lipid-packing density, *i.e.* reduced membrane rigidity (53). Increased spontaneous curvature and less density/rigidity may facilitate the focal outfoldings in myelin observed in the NECL4$^{-/-}$ mouse (9). Interestingly, Schwann cell membranes in the SREBP cleavage activation protein (SCAP) null mice are abundant in unsaturated lipids and abnormal in myelin membrane packing (54).

We noticed a particular increase in phosphatidylcholine species featuring very long polyunsaturated fatty acid chains (Fig. 4*A*) such as PtdCho-38:4 (18:0/20:4), PtdCho-38:5 (18:1/20:4), or PtdCho-38:6 (18:2/20:4; 16:0/22:6). These are hallmarks of phosphatidylcholine species synthesized through the PEMT pathway (47, 48). Interestingly, the PEMT pathway is up-regulated in the liver of rats that are fed a choline-deficient diet (55). The PEMT pathway has long been associated with hepatic cells, in which it accounts for about 30% of phosphatidylcholine synthesis, which through the activity of phosphatidylcholine-specific phospholipases C and/or D can generate choline *de novo*. However, PEMT increased activity during long periods of choline deficiency is not sufficient to fully compensate choline deficits. Therefore, assuming that the increase in very long chain-PUFA does reflect an increase in PEMT activity in NECL4-deficient Schwann cells, it remains to be determined whether the PEMT pathway in Schwann cells would be suffi-

cient to drive the overall 50% increase in total phosphatidylcholine and choline.

Albeit at a lower level, PEMT is present in non-hepatic tissues in which choline metabolism is important, particularly in the brain (56–58), where it has been shown to exhibit strong increases in activity during development and remyelination. For example, PEMT activity is increased 2–4-fold in the developing brain of neonatal rats, compared with adult brain. This increase is observed between the 5th and 20th postnatal days (57), which correspond in rodents to the period of active myelin formation in the CNS (59, 60). Brain PEMT activity is also dramatically increased (87-fold) after 7 days of remyelination following a 6-week cuprizone treatment (58) as well as in diabetic mice (10-fold) (58). Tashiro *et al.* (57) have hypothesized that this PEMT activity may be, in part, necessary for the repair of damaged myelin.

Interestingly, using two independent antibodies, we showed that PEMT is expressed in myelinating sciatic nerves (*i.e.* PNS), particularly during the early stages of myelination (P0 to P7) and that, at least in isolated cells, the expression is restricted to Schwann cells (Fig. 4). The timing of expression is intriguing, as it corresponds to the period of abundant plasma membrane formation and extension by Schwann cells to sort out axons and form the myelin sheath in the PNS. It is an interesting and novel finding that may indicate a contribution of PEMT-derived lipid during axonal sorting and wrapping, where the demand for lipids for the expanding plasma membrane is high (61).

We also observed an increase in the levels of phosphatidylinositols (Fig. 5), particularly species with fatty acids chains totaling 34 and 36 carbons and carrying two and three unsaturations. No phosphatidylinositols with completely saturated fatty acid chains were detected. Phosphorylated phosphatidylinositols are difficult to ionize, and we were unfortunately not able to further our analysis to species such as PIP_3, relevant to the ensheathing/myelinating phenotype transition, as well as myelin thickness in the PNS, and $PI(3,5)P_2$, relevant to the Charcot-Marie-Tooth type 4B-like phenotype observed in the NECL4 knock-out mouse. These phosphorylated phosphatidylinositols represent cytosolic docking sites for the activation of signaling pathways and the regulation of vesicular trafficking (61). Regulation is provided by the concurrent and opposing actions of phosphatidylinositol kinases (*e.g.* PI3K) and phosphatidylinositol phosphatases (*e.g.* PTEN, MTMR2). An enrichment in the $PI(3,4,5)P_3$ species could result in the hyperstimulation of the PI3K/AKT pathway and promote the focal hyper-myelination and aberrant myelin outfoldings observed in the $NECL4^{-/-}$ mouse. Indeed, myelinating Schwann cells lacking phosphatase and tensin (PTEN) homolog, a lipid phosphatase that dephosphorylates $PI(3,4,5)P_3$ to $PI(4,5)P_2$, exhibit tomacula and focal hyper-myelination (27). Selective ablation of the myotubularin-related 2 (MTMR2) in Schwann cells results in a similar phenotype to the $NECL4^{-/-}$ mouse, characterized by aberrant myelin outfoldings (31). MTMR2 is a phosphatidylinositol-3-phosphatase involved in the tight regulation of $PI(3,5)P_2$, suggesting that elevated levels of $PI(3,5)P_2$ may be involved in the observed phenotype.

Finally, we also noted a decrease in the activation of AKT in NECL4-deficient Schwann cells, as measured by the ratio of phospho-AKT (p-AKT) to total AKT (t-AKT). Interestingly, a similarly decreased ratio of p-AKT to t-AKT was observed in the *Mtmr2/Mtmr13* double knock-out mouse (62). However, the actual levels of phospho-AKT in the *Mtmr2/Mtmr13* double knock-out mouse are comparable with controls, whereas the levels of total AKT are elevated, hence the decreased ratio of p-AKT to t-AKT. In this study, the reduction in phospho-AKT levels is responsible for the decreased p-AKT to t-AKT ratio. The activation of ERBB2 and ERBB3 was not affected, suggesting that Nrg1 binding to ERBB3, recruitment of ERBB2, and ERBB activation were not perturbed by the absence of NECL4 in Schwann cells, and therefore they do not explain the deficit in AKT activation. AKT is positively regulated by its interaction with $PI(3,4,5)P_3$ and $PI(3,4)P_2$ (63). AKT can also interact with other phosphorylated phosphatidylinositols, albeit at a lower affinity, which, however, do not increase its activation (63). In fact, it was shown that excess of $PI(3,4,5)P_3$ reduced AKT autophosphorylation (63). It is therefore possible that the dysregulation of the phosphatidylinositols observed in the NECL4-deficient Schwann cells leads to a dysregulation of AKT activation. Future studies will be needed to determine whether the increase in phosphatidylinositols in the NECL4-deficient Schwann cells affects the profile of downstream phosphorylated phosphatidylinositol species. It is interesting to note, however, that the decrease in phospho-AKT may correlate with the delay in myelination onset that is observed in the $NECL4^{-/-}$ mouse (9).

Little is known about the molecular mechanisms involved in the regulation of the lipid synthesis that is needed to account for the rapidly expanding plasma membrane that will eventually compact to form the myelin sheath (3), without affecting structure and signaling pathways. It is likely, however, that axo-glial interaction is involved. For example, it was shown that soluble neuregulin-1 up-regulates in cultured Schwann cells the transcription of 3-hydroxy-3-methylglutaryl-CoA reductase, the rate-limiting enzyme in the biosynthesis of cholesterol, one of the major lipids of Schwann cell membrane and of the myelin sheath (64). This activation is dependent on the PI3K pathway, a pro-myelinating pathway in the context of PNS myelination. It has therefore been proposed that activation of the ERBB/PI3K cascade in Schwann cells by axonal contact mediates plasma membrane expansion through increased cholesterol synthesis (64). Choline-derived lipids represent another major group of myelin sheath lipids. It is therefore interesting that another component involved in axo-glial interactions, Schwann cell-specific NECL4, is found to interact with the choline transporter CTL1. Our data clearly show the impact of NECL4 deficiency on choline homeostasis, as well as a quantitative and qualitative impact on choline-dependent phospholipids such as phosphatidylcholine and phosphatidylinositol. These results further lend support to the hypothesis for a regulation of lipid biogenesis by axo-glial interaction during the process of myelination. This study also shed lights on the CTL family of choline transporters. There are five genes, each encoding several splice variants (65), underscoring the importance of choline intake regulation, which may be specific to a cell type and/or specific to a biosynthetic pathway (42, 65, 66). The failure of CTL1-deficient Schwann cells to form MBP^+

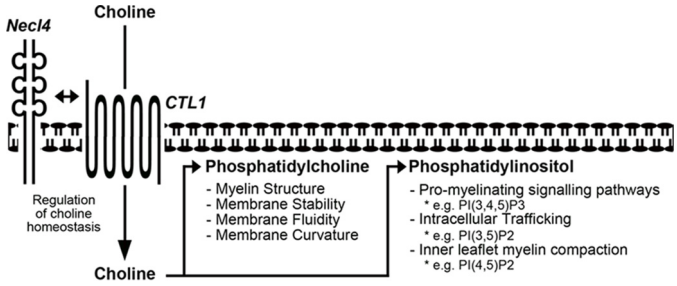

FIGURE 8. **Schematic summary of how NECL4 deficiency in Schwann cells may, by interacting with CTL1, impact myelination.** Dysregulation of homeostatic levels of choline, phosphatidylcholines, and phosphatidylinositols, as well as fatty acid chains length and unsaturation, may result in disruptions to myelin structure, membrane stability and curvature, and pro-myelinating signaling pathways.

myelin segments to control levels (Fig. 7) definitely suggests a role for choline transport through CTL1 in the process of myelination.

These studies are currently *in vitro* studies. However, they outline a potential molecular mechanism by which NECL4 may regulate PNS myelination. Fig. 8 summarizes how NECL4 deficiency in Schwann cells may, by affecting choline homeostasis, impact myelination. It will be important to translate these results *in vivo*, in particular by a detailed lipidomic analysis of the NECL4$^{-/-}$ mouse. Further studies on choline transporters and regulation in the context of myelination would also be informative. Finally, the mechanism(s) underlying NECL4 function in regulating CTL1 levels and choline transport in Schwann cells need to be clarified. Possible mechanisms include the targeting of CTL1 to the plasma membrane, the regulation of its stability, or regulation of CTL1 in transporting choline directly.

Experimental Procedures

Antibodies and Growth Factors—Antibodies were used at 1:1000 dilution unless otherwise stated. Primary antibodies are as follows: mouse anti-NECL4 (BioLegend catalog no. 833301, lot no. 437-4VA-37); goat anti-NECL4 (Origene, catalog no. TA303285, lot no. E060508); mouse anti-CTL1 (1:250; Novus catalog no. H00023446-A01, lot no. F4021); mouse anti-V5 (GeneScript catalog no. A01724, lot no. 13B000570); mouse anti-THY1.1 (AbD Serotec catalog no. MCA04G, lot no. 1014); chicken anti-GFP (Aves catalog no. GFP-1010, lot no. 0511FP12); rabbit polyclonal anti-PEMT (Abnova, catalog no. H00010400-D01P, lot no. G7211; full-length PEMT epitope); rabbit monoclonal anti-PEMT (Abcam, catalog no. MABN1145, lot no. Q2476316; C-terminal epitope); mouse anti-myelin basic protein (1:250; MBP; Covance catalog no. SMI-94R, lot no. D13CF00661); chicken anti-P0 (Millipore, AB9353, lot no. NMM1740754); phosphorylated AKT$^{Ser\text{-}473}$ (Cell Signaling Technologies, catalog no. 4057, lot no. 13); total AKT (Cell Signaling Technologies, catalog no. 9272, lot no. 25); phosphorylated ERBB3$^{Tyr\text{-}1289}$ (Cell Signaling Technologies, catalog no. 4791, lot no. 15); total ERBB3 (NeoMarkers, catalog no. MS-201-P1, lot no. 01P1408J); phosphorylated ERBB2$^{Tyr\text{-}1248}$ (Santa Cruz Biotechnology, catalog no. SC12352, lot no. G0213); and total ERBB2 (Santa Cruz Biotechnology, catalog no. SC284, lot no. H0906). Secondary antibodies are as follows: donkey anti-mouse Alexa 488 (Jackson ImmunoResearch, catalog no. 715-545-151, lot no. 125268); donkey anti-mouse rhodamine-X (Jackson ImmunoResearch, catalog no. 715-295-151, lot no. 126823); donkey anti-chicken Alexa 488 (Jackson ImmunoResearch, catalog no. 703-545-155, lot no. 125269); donkey anti-goat rhodamine-X (Jackson ImmunoResearch, catalog no. 705-295-147, lot no. 128297); goat anti-mouse Alexa 790 (light-chain specific; Jackson ImmunoResearch, catalog no. 115-655-174, lot no. 114402); donkey anti-rabbit Alexa 790 (Jackson ImmunoResearch, catalog no. 711-655-152, lot no. 125990); and donkey anti-chicken Alexa 790 (Jackson ImmunoResearch, catalog no. 703-655-155, lot no. 106150). Growth factors used are as follows: EGF domain of recombinant human NRG1β1 (EGF-D, R&D Systems 396-HB) and neural growth factor (NGF; AbD Serotec PMP04Z).

Culture Media—The media used are as follows: DMEM (Gibco 11995); neurobasal media (Gibco 21103); minimum Eagle's medium (Gibco 11090); Leibovitz's L-15 medium (Gibco 11415); fetal bovine serum (FBS; Gibco 16000); GlutaMax^{TM}-I (Gibco 35050); forskolin (Sigma F6886); B27 supplement (Gibco 17504); glucose (Sigma G7528); cytosine-β-arabinofuranoside hydrochloride (Sigma C6645); fluorodeoxyuridine (Sigma F0503); uridine (Sigma U3750); Matrigel (growth factor reduced; Corning 354230);and poly-L-lysine (Sigma P4707).

Animals and Cell Cultures—Sprague-Dawley rats (Hilltop Lab Animals) were housed and cared for in accordance with an animal protocol approved by Rutgers University Institutional Animal Care and Use Committee. Rat Schwann cell cultures were established from sciatic nerves as described previously (73). Primary Schwann cells were plated to poly-L-lysine (100 μg/ml)-coated plates in Schwann cell media (DMEM, 10% FBS, 2 mM GlutaMax^{TM}-I). Arabinofuranoside hydrochloride was applied for 3 days to remove contaminating fibroblasts. Cells were expanded in the aforementioned culture media with EGF-D (10 ng/ml) and forskolin (2 μM) until use. For neuron cultures, DRG were isolated from E15 embryos and plated to Matrigel-coated coverslips (300 μg/ml) in neuron culture media (Neurobasal media, 50 ng/ml NGF, 2% B27, 1% GlutaMax^{TM}-I, 0.08% glucose). Non-neural cells were eliminated by alternate feeding with media containing fluorodeoxyuridine and uridine (10 μM each) and then kept in neuron culture media until use (2 weeks).

RNA Interference of CTL1 and NECL4 Expression in Schwann Cells—Two 21-nucleotide-long shRNAs (shCTL1A, gcattgggatgggatttattt, and shCTL1B, gatacgacagctatggaaata) targeting CTL1 at positions 126–147 and 192–213, respectively (GenBank^{TM} accession number NM_001033852.1), were designed using the following on-line tool: BLOCK-iT RNAi designer (Invitrogen). The shRNAs against NECL4 were described in Ref. 8. The shRNA stem loops consisted of a sense shRNA sequence followed by a short nonspecific loop sequence (TTCAAGAGA) and the reverse/complement antisense shRNA sequence, followed by six thymidines that serve as a stop signal for the RNA polymerase III. The oligonucleotides were cloned into the HpaI-XhoI sites of the pLentiLox pLL3.7 lentiviral vector (Addgene, plasmid 11795), in which the U6 promoter drives the expression of

the shRNA, and the GFP marker is expressed under a CMV promoter (49). The lentiviral constructs were transfected into 293FT cells, together with packaging plasmids pMD2.G (Addgene plasmid 12259) and psPAX2 (Addgene plasmid 12260), by $CaPO_4$-mediated transfection (Invitrogen K278001). We used a pLL3.7 construct encoding an shRNA against luciferase as a control for nonspecific effects. Viral supernatants were collected 48 h after transfection and centrifuged at 1,600 × *g* for 20 min to pellet cell debris. Viral particles were concentrated (Lenti-X Concentrator kit; Clontech 631231) and either used immediately, or aliquoted and frozen (−80 °C) for later use. For the infection, Schwann cells at passage 2 were treated with viral particles prepared in Schwann cell media supplemented with EGF-D and forskolin 24 h after plating the cells. The following day, cells were fed with fresh media and used after 5 days, by which time knockdown was effective.

Myelination Assay—Schwann cells (±lentiviral infection) were plated to DRG cultures (1×10^5 per coverslip) and maintained in co-culture media (minimum Eagle's medium, 10% FBS, 50 ng/ml NGF, 0.4% glucose) for 3 days to allow Schwann cells to associate with neurites. Ascorbic acid (50 μg/ml) was subsequently added to promote myelin formation. Media were changed every other day for 10 days before cultures were immunostained for MBP.

Intracellular Signaling Assay—The ERBB/PI3K/AKT pathway in control, NECL4-deficient, and NECL4-rescued Schwann cells was activated via incubation (10 min, 37 °C) with a recombinant protein including the C-terminal EGF-like domain of type III neuregulin 1 (rhSMDF; R&D Systems catalog no. 378-SM). Whole cell lysates were immunoblotted for activated (phosphorylated) and total ERBB2, ERBB3, and AKT. Ratios of phosphoprotein to total protein were compared between (shLuc) control, NECL4-deficient, and NECL4-rescued Schwann cells.

qRT-PCR—RNA from sciatic nerve (embryonic day E18 to postnatal day P21) was extracted with TRIzol reagent (Invitrogen catalog no. 15596), and cDNA was generated with the SuperScript III first-strand synthesis kit (Invitrogen catalog no. 18080051). Specific targets were amplified by qRT-PCR performed on a LightCycler 480 II (Roche Applied Science) using the Maxima SYBR Green/ROX qRT-PCR master mix (Thermo Fisher Scientific catalog no. K0221). Primers were designed using the web version of the Primer3 software (74, 75) and the rat genome assembly version Rnor_6.0. Forward (Fwd) and reverse (Rev) primer pairs were selected to amplify targets overlapping splice junctions at the position of long introns to minimize amplifications from pre-mRNA-derived cDNAs. First pair is overlap exons 14–15: Fwd 5′-cctagtcgctcattgcttcc, and Rev 5′-gcctcccttaccagcttctt; and second pair is overlap exons 13–14: Fwd 5′-caccaacttctgcacctcag, and Rev 5′-ggaagcaatgagcgactagg. Melting point (T_m) curve analysis was performed on all qRT-PCRs to verify the detection of a unique peak for each reaction, at the expected T_m. All end point reactions were separated on a 15% DNA polyacrylamide gel to confirm the detection of a unique amplicon of the expected size (236 bp).

Co-immunoprecipitation—Schwann cells were incubated for 45 min at room temperature in cell-permeable chemical cross-linker 2 mM DSP (Thermo Fisher Scientific catalog no. 22585) in 25 mM HEPES (pH 7.4), 150 mM NaCl, 13 mM NaOH, with gentle agitation. Cross-linking was quenched in 1 M Tris-HCl (pH 7.4) with L-cysteine (Sigma) (67) before cell lysis in RIPA Buffer (Thermo Fisher Scientific catalog no. 89901). Lysates of four inner diameter 100-mm confluent plates were pooled and centrifuged at 10,000 × *g* to remove cell debris. After protein estimation (BCA kit, Pierce catalog no. 23228), the supernatant (250 μg of proteins in 1 ml) was pre-cleared (3 h, room temperature) before overnight incubation (4 °C) with 5 μg of antibody against NECL4 and agarose-protein G beads (Thermo Fisher Scientific catalog no. 22852). Protein complexes were dissociated from beads by (i) boiling (100 °C) for 30 min without reducing agent to maintain the integrity of the chemical cross-links (Fig. 1*A*) (67) or (ii) incubating in the presence of DTT reducing agent (70 °C for 10 min) to cleave chemical cross-links. Supernatant was collected for Western blotting and mass spectrometry analyses. For NECL4/CTL1 reciprocal coIPs (Fig. 1*D*), antibodies for NECL4 or CTL1 (5 μg) were incubated with agarose-protein G beads in non-cross-linked cell lysates overnight at 4 °C. Bound beads were incubated in the presence of DTT reducing agent (70 °C for 10 min) before Western blotting analysis on protein lysate.

Western Blotting—Reduced/non-reduced lysates were loaded to BisTris gels (1 M BisTris (pH 7.4), 10% acrylamide/bisacrylamide, 1% ammonium persulfate, 0.15% TEMED) and run in MOPS buffer (Boston BioProducts, catalog no. BP-178). Gels were either stained with Oriole gel stain (Bio-Rad, catalog no. 161-0496; as per the manufacturer's instructions) or transferred to 0.22 μM nitrocellulose membrane (Bio-Rad, catalog no. 162-0252) and blotted for desired candidates.

Proteomic MS—Non-reduced protein complexes were excised from gel (Fig. 1*A*), and proteomic MS was performed on commission at the Center for Advanced Proteomics Research, Rutgers University. The MASCOT search engine (version 2.3; Proteome Discoverer platform version 1.3; Thermo Fisher Scientific) was used for protein identification. Searches were restricted to rat sequences in the UniRef database. Scaffold software (version 4.4.1; using the X!Tandem (43)) and ProteinProphet computer algorithms (45) were used under license to quantify proteomic mass spectrometry data. Probabilistic validation of peptides was achieved using PeptideProphet (44), with identified peptides solely used for analysis.

Immunocytochemistry of Teased Fibers and Myelinated Co-cultures—Sciatic nerves were collected from 30-day-old rats. Epineurial tissue was removed before fixation in 4% PFA for 2 h at 4 °C. Nerves were manually teased with fine needles, mounted to glass slides, dried overnight at room temperature, and stored at −80 °C until use (8). For immunocytochemistry staining of NECL4, the teased fibers were permeabilized in 100% methanol (−20 °C for 20 min.), and for CTL1 staining, the fibers were permeabilized with 0.5% Triton X-100 in PBS. After blocking (5% BSA, 1% donkey serum, in PBS) for 1 h at room temperature, fibers were incubated with primary antibodies (mouse anti-NECL4, mouse anti-CTL1, both at 1:250; chicken anti-P0 at 1:3,000) overnight at 4 °C. Detection of NECL4 and CTL1 was done with a rhodamine-X-conjugated anti-mouse secondary antibody, whereas P0 was detected with an Alexa

488-conjugated anti-chicken secondary. All secondaries were used at 1:250 for 2 h at room temperature.

Schwann cell monocultures and myelinating co-cultures were fixed in 4% PFA (15 min, room temperature), permeabilized in 100% methanol (−20 °C for 20 min.), blocked, and incubated with relevant antibodies (anti-V5, 1:250; anti-GFP, 1:1000; anti-MBP, 1:250; overnight at 4 °C). Primary antibodies were detected with the appropriate secondaries at 1:250 for 2 h at room temperature. Schwann cell nuclei were stained for 10 min with DAPI prepared in PBS.

Co-clustering of NECL4 and CTL1—Live Schwann cell cultures were incubated consecutively with goat anti-NECL4 primary antibody and rhodamine-X-conjugated secondary antibody (each 1:250, room temperature, 45 min). Cells were then washed three times with 500 μl of ice-cold PBS, fixed with 4% PFA in PBS (15 min, room temperature), and permeabilized with 0.5% Triton X-100 in blocking solution (1 h at room temperature). CTL1 was then detected by incubating the fixed cells first with the mouse anti-CTL1 (1:250, 4 °C overnight) and then with the Alexa 488 anti mouse secondary (1:250, 1 h at room temperature). Cultures were washed in PBS and Schwann cell nuclei stained with DAPI.

Microscopy—All cultures and sciatic nerve fibers for immunofluorescence analysis and image capture were mounted in anti-fading agent Citifluor (Ted Pella 19472). Fluorescent images (Figs. 2*B* and 7, *A* and *C*) were captured at room temperature on a Nikon Eclipse TE2000 microscope (×20/0.75 and ×40/1.30) with a Hamamatsu Photonics camera (model C4742-95-12ERG) using MetaMorph software (Universal Imaging Corp.). Images for Fig. 1*E* were captured on a Zeiss LSM 510NLD Meta laser scanning multiphoton confocal microscope (×40/1.3; Carl Zeiss microImaging). Images for Fig. 1*G* were captured on a Zeiss Cell Observer SD confocal system (×63/1.4 with ×1.6 tube lens magnification; Carl Zeiss microImaging).

Lipidomics, Assays for Endogenous Choline and Uptake of d_9-Choline—For assessment of intracellular choline, control and knockdown Schwann cells were detached via trypsin/EDTA digestion and flooded with ice-cold Hanks' balanced salt solution (without serum). Cell counts were established (averaged from three individual counts) for all treatment groups before lipid extraction. To assess the amount of intracellular deuterated d_9-choline after uptake from the extracellular compartment, 2–3 × 10^5 cells were incubated in 130 μM d_9-choline (in 1.5 mM $CaCl_2$, 1.3 mM $MgSO_4$, 1.8 g/liter glucose) for 6 min at 37 °C. Ice-cold PBS was added, and cells were immediately transferred to ice before lipid extraction.

Lipid Extraction—Lipid extraction was performed on ice via established protocols (68) with minor revisions. Cellular H^+/Na^+/K^+ ions were exchanged for ice-cold 100 mM cesium chloride (Cs^+) before resuspension and extensive sonication in methanol. Methanol-suspended lipids were isolated from the pelleted material for MALDI-TOF and lipidomic mass spectrometry analysis.

MALDI-TOF—50 μM deuterated choline standard (d_9- or d_4-choline; Cambridge Isotopes Labs, catalog nos. DLM-5491 and CDLM-8914-PK, respectively) was added to freshly made common matrix (10 mg/ml (w/v) ferulic acid (single isotope version; Sigma catalog no. 46278)), 30% acetonitrile (v/v; Sigma catalog no. 34967), 0.1% trifluoroacetic acid (Sigma catalog no. 302031 (69)) before mixing with equal volumes of methanol-suspended lipids samples and spotting (2 μl) to MALDI-TOF plates. Assessment of intracellular choline (m/z 104), d_4-choline (m/z 108), and d_9-choline (m/z 113) was made on a 4800 Plus MALDI TOF/TOF analyzer using the "linear positive low mass" setting, and with the 4000 series version 3.7.0 software (ABSciex Corp.). Individual spectra were established from averages of 5,000 individual laser readings, of 4–8 spots per sample. Areas under each spectral peak (intracellular endogenous choline or d_9-choline after uptake, Fig. 2) were compared with areas of standard spectral peaks (d_9-choline and d_4-choline, respectively, Fig. 2) for inter-sample comparative analysis. Areas under spectral peaks were established using the Data Explorer software (version 3.2.3).

Lipidomic Mass Spectrometry—Electrospray ionization mass spectrometry (ESI-MS; LipoSpectrum, St Louis, MO) was employed to measure femtomole to picomole concentrations of phosphatidylcholine, diacylglycerol, phosphatidylinositol, and sphingomyelin species (LipoSpectrum, as described previously (70)). Quadrupole 1 thresholds were set to analyze ions within specific m/z ratios within each lipid species. Raw lipid concentrations were adjusted for both protein concentration and cell number to give pmol/10^6 Schwann cells. An arbitrary threshold of >0.5% (depending on signal quality) was assigned to remove noise.

Data/Statistical Analysis and Computer Software—To control for the possible contribution of the lipids, or effects attributable to expression of an shRNA, we compared shNECL4 (* rescue) to control cells infected with shLuc (instead of wild type cells) for analysis. Statistical analysis (one-way analysis of variance for independent samples with Tukey HSD post-hoc test) was performed using the on-line VassarStats package.

Author Contributions—C. H. performed most of the experiments and data analysis and wrote the manuscript. M. R. J. performed initial MALDI-TOF experiments for Fig. 2. T. L. performed the proteomic mass spectrometry in Fig. 1. H. K. acquired and provided data for Fig. 1. K. B. contributed assistance in preparation of infected cells for Figs. 2–4. H. L. and M. R. J. helped with proteomic mass spectrometry and MALDI-TOF and data analysis. P. M. conceived the idea, coordinated the study, and wrote the manuscript with C. H.

Acknowledgments—We thank Dr. Haesun Kim for helpful discussion. We thank Dr. Baichen Zhang at LipoSpectrum Inc. for lipidomic mass spectrometry and Drs. Haiyan Zheng and Caifeng Zhao (Rutgers University) for help with MALDI-TOF mass spectrometry. Operation of the Center for Advanced Proteomics was supported by National Institutes of Health Grant P30 NS046593 from NINDS (to H. L.).

References

1. Bunge, R. P., Bunge, M. B., and Bates, M. (1989) Movements of the Schwann cell nucleus implicate progression of the inner (axon-related) Schwann cell process during myelination. *J. Cell Biol.* **109,** 273–284
2. Gould, R. M. (1977) Incorporation of glycoproteins into peripheral nerve myelin. *J. Cell Biol.* **75,** 326–338
3. Webster, H. D. (1971) The geometry of peripheral myelin sheaths during their formation and growth in rat sciatic nerves. *J. Cell Biol.* **48,** 348–367

4. Guidotti, G. (1972) Membrane proteins. *Annu. Rev. Biochem.* **41,** 731–752
5. Campagnoni, A. T., and Campagnoni, C. W. (2004) in *Myelin Biology and Disorders* (Lazzarini, R. A., ed) pp. 387–400, Elsevier/Academic Press, San Diego
6. Hudson, L. D. (2004) in *Myelin Biology and Disorders* (Lazzarini, R. A., ed) pp. 387–401-420, Elsevier/Academic Press, San Diego
7. Kirschner, D. A., Wrabetz, L., and Feltri, M. L. (2004) in *Myelin Biology and Disorders* (Lazzarini, R. A., ed) pp. 523–545, Elsevier/Academic Press, San Diego
8. Maurel, P., Einheber, S., Galinska, J., Thaker, P., Lam, I., Rubin, M. B., Scherer, S. S., Murakami, Y., Gutmann, D. H., and Salzer, J. L. (2007) Nectin-like proteins mediate axon Schwann cell interactions along the internode and are essential for myelination. *J. Cell Biol.* **178,** 861–874
9. Golan, N., Kartvelishvily, E., Spiegel, I., Salomon, D., Sabanay, H., Rechav, K., Vainshtein, A., Frechter, S., Maik-Rachline, G., Eshed-Eisenbach, Y., Momoi, T., and Peles, E. (2013) Genetic deletion of CADM4 results in myelin abnormalities resembling Charcot-Marie-Tooth neuropathy. *J. Neurosci.* **33,** 10950–10961
10. Spiegel, I., Adamsky, K., Eshed, Y., Milo, R., Sabanay, H., Sarig-Nadir, O., Horresh, I., Scherer, S. S., Rasband, M. N., and Peles, E. (2007) A central role for NECL4 (SynCAM4) in Schwann cell-axon interaction and myelination. *Nat. Neurosci.* **10,** 861–869
11. Yageta, M., Kuramochi, M., Masuda, M., Fukami, T., Fukuhara, H., Maruyama, T., Shibuya, M., and Murakami, Y. (2002) Direct association of TSLC1 and DAL-1, two distinct tumor suppressor proteins in lung cancer. *Cancer Res.* **62,** 5129–5133
12. Zhou, Y., Du, G., Hu, X., Yu, S., Liu, Y., Xu, Y., Huang, X., Liu, J., Yin, B., Fan, M., Peng, X., Qiang, B., and Yuan, J. (2005) Nectin-like molecule 1 is a protein 4.1N associated protein and recruits protein 4.1N from cytoplasm to the plasma membrane. *Biochim. Biophys. Acta* **1669,** 142–154
13. Fujita, E., Tanabe, Y., Hirose, T., Aurrand-Lions, M., Kasahara, T., Imhof, B. A., Ohno, S., and Momoi, T. (2007) Loss of partitioning-defective-3/isotype-specific interacting protein (par-3/ASIP) in the elongating spermatid of RA175 (IGSF4A/SynCAM)-deficient mice. *Am. J. Pathol.* **171,** 1800–1810
14. Jang, W. H., Choi, S. H., Jeong, J. Y., Park, J. H., Kim, S. J., and Seog, D. H. (2014) Neuronal cell-surface protein neurexin 1 interaction with multi-PDZ domain protein MUPP1. *Biosci. Biotechnol. Biochem.* **78,** 644–646
15. Kakunaga, S., Ikeda, W., Itoh, S., Deguchi-Tawarada, M., Ohtsuka, T., Mizoguchi, A., and Takai, Y. (2005) Nectin-like molecule-1/TSLL1/SynCAM3: a neural tissue-specific immunoglobulin-like cell-cell adhesion molecule localizing at non-junctional contact sites of presynaptic nerve terminals, axons and glia cell processes. *J. Cell Sci.* **118,** 1267–1277
16. Tanford, C. (1978) The hydrophobic effect and the organization of living matter. *Science* **200,** 1012–1018
17. Kennedy, E. P., and Weiss, S. B. (1956) The function of cytidine coenzymes in the biosynthesis of phospholipids. *J. Biol. Chem.* **222,** 193–214
18. Lassègue, B., Alexander, R. W., Clark, M., Akers, M., and Griendling, K. K. (1993) Phosphatidylcholine is a major source of phosphatidic acid and diacylglycerol in angiotensin II-stimulated vascular smooth-muscle cells. *Biochem. J.* **292,** 509–517
19. Athenstaedt, K., and Daum, G. (1999) Phosphatidic acid, a key intermediate in lipid metabolism. *Eur. J. Biochem.* **266,** 1–16
20. Tafesse, F. G., Ternes, P., and Holthuis, J. C. (2006) The multigenic sphingomyelin synthase family. *J. Biol. Chem.* **281,** 29421–29425
21. Coetzee, T., Fujita, N., Dupree, J., Shi, R., Blight, A., Suzuki, K., Suzuki, K., and Popko, B. (1996) Myelination in the absence of galactocerebroside and sulfatide: normal structure with abnormal function and regional instability. *Cell* **86,** 209–219
22. Owens, G. C., and Bunge, R. P. (1990) Schwann cells depleted of galactocerebroside express myelin-associated glycoprotein and initiate but do not continue the process of myelination. *Glia* **3,** 118–124
23. Nadra, K., de Preux Charles, A. S., Médard, J. J., Hendriks, W. T., Han, G. S., Grès, S., Carman, G. M., Saulnier-Blache, J. S., Verheijen, M. H., and Chrast, R. (2008) Phosphatidic acid mediates demyelination in Lpin1 mutant mice. *Genes Dev.* **22,** 1647–1661
24. Michailov, G. V., Sereda, M. W., Brinkmann, B. G., Fischer, T. M., Haug, B., Birchmeier, C., Role, L., Lai, C., Schwab, M. H., and Nave, K. A. (2004) Axonal neuregulin-1 regulates myelin sheath thickness. *Science* **304,** 700–703
25. Taveggia, C., Zanazzi, G., Petrylak, A., Yano, H., Rosenbluth, J., Einheber, S., Xu, X., Esper, R. M., Loeb, J. A., Shrager, P., Chao, M. V., Falls, D. L., Role, L., and Salzer, J. L. (2005) Neuregulin-1 type III determines the ensheathment fate of axons. *Neuron* **47,** 681–694
26. Cotter, L., Ozçelik, M., Jacob, C., Pereira, J. A., Locher, V., Baumann, R., Relvas, J. B., Suter, U., and Tricaud, N. (2010) Dlg1-PTEN interaction regulates myelin thickness to prevent damaging peripheral nerve overmyelination. *Science* **328,** 1415–1418
27. Goebbels, S., Oltrogge, J. H., Wolfer, S., Wieser, G. L., Nientiedt, T., Pieper, A., Ruhwedel, T., Groszer, M., Sereda, M. W., and Nave, K. A. (2012) Genetic disruption of Pten in a novel mouse model of tomaculous neuropathy. *EMBO Mol. Med.* **4,** 486–499
28. Fitzner, D., Schneider, A., Kippert, A., Möbius, W., Willig, K. I., Hell, S. W., Bunt, G., Gaus, K., and Simons, M. (2006) Myelin basic protein-dependent plasma membrane reorganization in the formation of myelin. *EMBO J.* **25,** 5037–5048
29. Musse, A. A., Gao, W., Homchaudhuri, L., Boggs, J. M., and Harauz, G. (2008) Myelin basic protein as a "PI(4,5)P2-modulin": a new biological function for a major central nervous system protein. *Biochemistry* **47,** 10372–10382
30. Nawaz, S., Kippert, A., Saab, A. S., Werner, H. B., Lang, T., Nave, K. A., and Simons, M. (2009) Phosphatidylinositol 4,5-bisphosphate-dependent interaction of myelin basic protein with the plasma membrane in oligodendroglial cells and its rapid perturbation by elevated calcium. *J. Neurosci.* **29,** 4794–4807
31. Bolis, A., Coviello, S., Bussini, S., Dina, G., Pardini, C., Previtali, S. C., Malaguti, M., Morana, P., Del Carro, U., Feltri, M. L., Quattrini, A., Wrabetz, L., and Bolino, A. (2005) Loss of Mtmr2 phosphatase in Schwann cells but not in motor neurons causes Charcot-Marie-Tooth type 4B1 neuropathy with myelin outfoldings. *J. Neurosci.* **25,** 8567–8577
32. Vaccari, I., Carbone, A., Previtali, S. C., Mironova, Y. A., Alberizzi, V., Noseda, R., Rivellini, C., Bianchi, F., Del Carro, U., D'Antonio, M., Lenk, G. M., Wrabetz, L., Giger, R. J., Meisler, M. H., and Bolino, A. (2015) Loss of Fig 4 in both Schwann cells and motor neurons contributes to CMT4J neuropathy. *Hum. Mol. Genet.* **24,** 383–396
33. Kim, T., and Pfeiffer, S. E. (1999) Myelin glycosphingolipid/cholesterol-enriched microdomains selectively sequester the non-compact myelin proteins CNP and MOG. *J. Neurocytol.* **28,** 281–293
34. Simons, M., Krämer, E. M., Thiele, C., Stoffel, W., and Trotter, J. (2000) Assembly of myelin by association of proteolipid protein with cholesterol- and galactosylceramide-rich membrane domains. *J. Cell Biol.* **151,** 143–154
35. Zacchetti, D., Peränen, J., Murata, M., Fiedler, K., and Simons, K. (1995) VIP17/MAL, a proteolipid in apical transport vesicles. *FEBS Lett.* **377,** 465–469
36. Simons, K., and van Meer, G. (1988) Lipid sorting in epithelial cells. *Biochemistry* **27,** 6197–6202
37. Verkade, P., and Simons, K. (1997) Robert Feulgen Lecture 1997. Lipid microdomains and membrane trafficking in mammalian cells. *Histochem. Cell Biol.* **108,** 211–220
38. Simons, K., and Toomre, D. (2000) Lipid rafts and signal transduction. *Nat. Rev. Mol. Cell Biol.* **1,** 31–39
39. Bazalakova, M. H., and Blakely, R. D. (2006) The high-affinity choline transporter: a critical protein for sustaining cholinergic signaling as revealed in studies of genetically altered mice. *Handb. Exp. Pharmacol.* 2006, 525–544
40. Meunier, F. M., and O'Regan, S. (2002) Expression of CTL1 in myelinating structures of *Torpedo marmorata*. *Neuroreport* **13,** 1617–1620
41. O'Regan, S., Traiffort, E., Ruat, M., Cha, N., Compaore, D., and Meunier, F. M. (2000) An electric lobe suppressor for a yeast choline transport mutation belongs to a new family of transporter-like proteins. *Proc. Natl. Acad. Sci. U.S.A.* **97,** 1835–1840
42. Traiffort, E., Ruat, M., O'Regan, S., and Meunier, F. M. (2005) Molecular characterization of the family of choline transporter-like proteins and their splice variants. *J. Neurochem.* **92,** 1116–1125

43. Craig, R., and Beavis, R. C. (2003) A method for reducing the time required to match protein sequences with tandem mass spectra. *Rapid Commun. Mass. Spectrom.* **17,** 2310–2316
44. Keller, A., Nesvizhskii, A. I., Kolker, E., and Aebersold, R. (2002) Empirical statistical model to estimate the accuracy of peptide identifications made by MS/MS and database search. *Anal. Chem.* **74,** 5383–5392
45. Nesvizhskii, A. I., Keller, A., Kolker, E., and Aebersold, R. (2003) A statistical model for identifying proteins by tandem mass spectrometry. *Anal. Chem.* **75,** 4646–4658
46. Bremer, J., and Greenberg, D. M. (1961) Methyl transferring enzyme system of microsomes in the biosynthesis of lecithin (phosphatidylcholine). *Biochim. Biophys. Acta* **46,** 205–216
47. DeLong, C. J., Shen, Y. J., Thomas, M. J., and Cui, Z. (1999) Molecular distinction of phosphatidylcholine synthesis between the CDP-choline pathway and phosphatidylethanolamine methylation pathway. *J. Biol. Chem.* **274,** 29683–29688
48. Ridgway, N. D., and Vance, D. E. (1988) Specificity of rat hepatic phosphatidylethanolamine *N*-methyltransferase for molecular species of diacyl phosphatidylethanolamine. *J. Biol. Chem.* **263,** 16856–16863
49. Rubinson, D. A., Dillon, C. P., Kwiatkowski, A. V., Sievers, C., Yang, L., Kopinja, J., Rooney, D. L., Zhang, M., Ihrig, M. M., McManus, M. T., Gertler, F. B., Scott, M. L., and Van Parijs, L. (2003) A lentivirus-based system to functionally silence genes in primary mammalian cells, stem cells and transgenic mice by RNA interference. *Nat. Genet.* **33,** 401–406
50. McGrath, M. C. (2016) Charcot-Marie-Tooth 1A: A narrative review with clinical and anatomical perspectives. *Clin. Anat.* **29,** 547–554
51. Macala, L. J., Yu, R. K., and Ando, S. (1983) Analysis of brain lipids by high performance thin-layer chromatography and densitometry. *J. Lipid Res.* **24,** 1243–1250
52. Szule, J. A., Fuller, N. L., and Rand, R. P. (2002) The effects of acyl chain length and saturation of diacylglycerols and phosphatidylcholines on membrane monolayer curvature. *Biophys. J.* **83,** 977–984
53. Talbot, W. A., Zheng, L. X., and Lentz, B. R. (1997) Acyl chain unsaturation and vesicle curvature alter outer leaflet packing and promote poly(ethylene glycol)-mediated membrane fusion. *Biochemistry* **36,** 5827–5836
54. Verheijen, M. H., Camargo, N., Verdier, V., Nadra, K., de Preux Charles, A. S., Médard, J. J., Luoma, A., Crowther, M., Inouye, H., Shimano, H., Chen, S., Brouwers, J. F., Helms, J. B., Feltri, M. L., Wrabetz, L., *et al.* (2009) SCAP is required for timely and proper myelin membrane synthesis. *Proc. Natl. Acad. Sci. U.S.A.* **106,** 21383–21388
55. Cui, Z., and Vance, D. E. (1996) Expression of phosphatidylethanolamine *N*-methyltransferase-2 is markedly enhanced in long term choline-deficient rats. *J. Biol. Chem.* **271,** 2839–2843
56. Vance, D. E. (2014) Phospholipid methylation in mammals: from biochemistry to physiological function. *Biochim. Biophys. Acta* **1838,** 1477–1487
57. Tashiro, S., Sudou, K., Imoh, A., Koide, M., and Akazawa, Y. (1983) Phosphatidylethanolamine methyltransferase activity in developing, demyelinating, and diabetic mouse brain. *Tohoku J. Exp. Med.* **141,** 485–490
58. Blusztajn, J. K., Zeisel, S. H., and Wurtman, R. J. (1985) Developmental changes in the activity of phosphatidylethanolamine *N*-methyltransferases in rat brain. *Biochem. J.* **232,** 505–511
59. Dangata, Y. Y., Findlater, G. S., and Kaufman, M. H. (1996) Postnatal development of the optic nerve in (C57BL x CBA)F1 hybrid mice: general changes in morphometric parameters. *J. Anat.* **189,** 117–125
60. Sturrock, R. R. (1980) Myelination of the mouse corpus callosum. *Neuropathol. Appl. Neurobiol.* **6,** 415–420
61. Stahelin, R. V., Scott, J. L., and Frick, C. T. (2014) Cellular and molecular interactions of phosphoinositides and peripheral proteins. *Chem. Phys. Lipids* **182,** 3–18
62. Berger, P., Tersar, K., Ballmer-Hofer, K., and Suter, U. (2011) The CMT4B disease-causing proteins MTMR2 and MTMR13/SBF2 regulate AKT signalling. *J. Cell. Mol. Med.* **15,** 307–315
63. Franke, T. F., Kaplan, D. R., Cantley, L. C., and Toker, A. (1997) Direct regulation of the AKT proto-oncogene product by phosphatidylinositol-3,4-bisphosphate. *Science* **275,** 665–668
64. Pertusa, M., Morenilla-Palao, C., Carteron, C., Viana, F., and Cabedo, H. (2007) Transcriptional control of cholesterol biosynthesis in Schwann cells by axonal neuregulin 1. *J. Biol. Chem.* **282,** 28768–28778
65. Yuan, Z., Tie, A., Tarnopolsky, M., and Bakovic, M. (2006) Genomic organization, promoter activity, and expression of the human choline transporter-like protein 1. *Physiol. Genomics* **26,** 76–90
66. Apparsundaram, S., Ferguson, S. M., George, A. L., Jr., and Blakely, R. D. (2000) Molecular cloning of a human, hemicholinium-3-sensitive choline transporter. *Biochem. Biophys. Res. Commun.* **276,** 862–867
67. Smith, A. L., Friedman, D. B., Yu, H., Carnahan, R. H., and Reynolds, A. B. (2011) ReCLIP (reversible cross-link immunoprecipitation): an efficient method for interrogation of labile protein complexes. *PLoS ONE* **6,** e16206
68. Estrada, V., Martínez-Larrad, M. T., González-Sánchez, J. L., de Villar, N. G., Zabena, C., Fernández, C., and Serrano-Ríos, M. (2006) Lipodystrophy and metabolic syndrome in HIV-infected patients treated with antiretroviral therapy. *Metabolism* **55,** 940–945
69. Baykal, A. T., Jain, M. R., and Li, H. (2008) Aberrant regulation of choline metabolism by mitochondrial electron transport system inhibition in neuroblastoma cells. *Metabolomics* **4,** 347–356
70. Ho, C. S., Lam, C. W., Chan, M. H., Cheung, R. C., Law, L. K., Lit, L. C., Ng, K. F., Suen, M. W., and Tai, H. L. (2003) Electrospray ionisation mass spectrometry: principles and clinical applications. *Clin. Biochem. Rev.* **24,** 3–12
71. van Helvoort, A., van't Hof, W., Ritsema, T., Sandra, A., and van Meer, G. (1994) Conversion of diacylglycerol to phosphatidylcholine on the basolateral surface of epithelial (Madin-Darby canine kidney) cells. Evidence for the reverse action of a sphingomyelin synthase. *J. Biol. Chem*. **269,** 1763–1769
72. Clarke, C. J., and Hannun, Y. A. (2006) Neutral sphingomyelins and nemeses: bridging the gaps. *Biochim. Biophys. Acta* **1758**, 1893–1901
73. Kim, H. A., and Maurel, P. (2010) in *Protocols for Neural Cell Culture* (Dowering, L. C., ed) pp. 253–268, Humana Press, New York
74. Koressaar, T., Remm, M. (2007) Enhancements and modifications of primer design program Primer3. *Bioinformatics* **23,** 1289–1291
75. Untergasser, A., Cucaracha, I., Koressaar, T., Ye, J., Faircloth, B. C., Remm, M., Rosen, S. G. (2012) Primer3–new capabilities and interfaces. *Nucleic Acids Res.* **40**, e115